Ecological Informatics 93 (2026) 103571

Contents lists available at ScienceDirect

Ecological Informatics

journal homepage: www.elsevier.com/locate/ecolinf

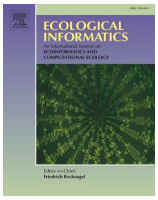

Open data analysis of terrestrial water storage and water availability in the Middle East: Spatiotemporal trends, hydroclimatic drivers, and socio-ecological implications

Fahimeh Youssefi [a,b], Behnam Khorrami [c], Shoaib Ali [d], Samira Sadat Soltani [e], Mohammad Javad Valadan Zoej [b], Jonathan Li [f], Ebrahim Ghaderpour [g,*]

[a] Institute of Artificial Intelligence, School of Mechanical and Electrical Engineering, Shaoxing University, 508 West Huancheng Road, Yuecheng District, Shaoxing, Zhejiang Province 312000, China
[b] Department of Photogrammetry and Remote Sensing, Faculty of Geodesy and Geomatics Engineering, K.N.Toosi University of Technology, Tehran, Iran
[c] Department of Remote Sensing & GIS, Faculty of Planning & Environmental Sciences, University of Tabriz, Tabriz, Iran
[d] Department of Earth and Space Sciences, Southern University of Science and Technology, Shenzhen 518005, China
[e] Institute of Bio- and Geosciences (IBG-3, Agrosphere), Forschungszentrum Jülich GmbH, 52425, Jülich, Germany
[f] Department of Systems Design Engineering, University of Waterloo, Waterloo, ON N2L 3G1, Canada
[g] Department of Earth Sciences and CERI Research Centre, University of Rome La Sapienza, Piazzale Aldo Moro, 5, RM 00185, Italy

ARTICLE INFO

Keywords:
Aridity
CHIRPS
Coherency
GLDAS-Noah
GRACE
Least-squares cross wavelet analysis
Remote sensing

ABSTRACT

This study examines the spatiotemporal variability of Terrestrial Water Storage (TWS) and Water Availability (WA) across the Middle East (ME) from 2002 to 2024 using exclusively open-access datasets, including GRACE/GRACE-FO mascon solutions, GLDAS-Noah simulations, CHIRPS precipitation records, and global aridity indices. The contributions of six hydroclimatic variables, such as snow water equivalent, canopy water storage, soil moisture storage, groundwater storage, precipitation, and evapotranspiration, to TWS and WA were quantified through component contribution ratio analysis and Least-Squares Cross Wavelet Analysis (LSCWA). The harmonized and reconstructed datasets provided here are openly accessible, enabling reproducibility and further regional water studies. Results reveal a critical decline in ME water storage, with an average depletion of −45 km^3 annually, and widespread WA deficits affecting about half the region. Groundwater storage emerged as the dominant contributor to TWS variability, particularly under arid and hyper-arid conditions, whereas soil moisture and snow water played stronger roles in humid zones. The coherency analysis indicates that annual cycles of TWS and WA were strongly linked with hydroclimatic drivers before 2020 but weakened in subsequent years. These findings, underpinned by openly shared datasets, provide essential resources and insights for water management strategies and sustainable policy development in one of the world's most water-stressed regions.

1. Introduction

The presence of water, both on the Earth's surface and underground, is of cardinal importance for the sustenance of human and wildlife populations, as well as for fostering economic and agricultural growth. This issue becomes more apparent when and where climate change and population growth necessitate more access to water to meet the needs (Ershadfath et al., 2024). The total water retained in glaciers, snowpacks, surface water bodies, including lakes, reservoirs, and wetlands, along with the moisture held in soils and vegetation canopies, as well as that contained in subterranean aquifers, is collectively referred to as Terrestrial Water Storage (TWS) (Rodell and Famiglietti, 2001). This comprehensive nature of TWS and its importance encourage researchers to obtain precise information on the variations of TWS over space and time to effectively monitor and manage the storage and availability of water. Despite the substantial progress achieved over the past 25 years through GRACE and GRACE-FO missions in characterizing global TWS dynamics, knowledge of its regional variability, component contributions, and interactions with hydroclimatic drivers remains limited, particularly for less-developed countries (such as the ME) where there is,

* Corresponding author.
E-mail addresses: youssefi@usx.edu.cn (F. Youssefi), bekhorram@tabrizu.ac.ir (B. Khorrami), engnr.shoaib.ali@gmail.com (S. Ali), s.soltani@fz-juelich.de (S.S. Soltani), valadanzouj@kntu.ac.ir (M.J. Valadan Zoej), junli@uwaterloo.ca (J. Li), ebrahim.ghaderpour@uniroma1.it (E. Ghaderpour).

https://doi.org/10.1016/j.ecoinf.2025.103571
Received 14 September 2025; Received in revised form 16 November 2025; Accepted 19 December 2025
Available online 20 December 2025

in general, an absence of global monitoring systems (Soltani et al., 2020, 2021). The progress of technology in space observation and remote sensing has provided us with the capability to access global data regarding changes in environmental parameters with a satisfactory level of accuracy (Arij et al., 2025). The initiation of the Gravity Recovery and Climate Experiment (GRACE) project has been a quantum leap in remote sensing of hydrology, aiming to observe changes in TWS on a global scale (Soltani et al., 2021).

The GRACE and GRACE Follow-on (GRACE-FO) missions (Tapley et al., 2019) have provided us with global observations of TWS variations and their data have so far been extensively used by many researchers to monitor Hydroclimatic events and variations of TWS and other water cycle components at local, regional and global domains (Forootan et al., 2014; Frappart and Ramillien, 2018; Tapley et al., 2019; Ali et al., 2021, 2022, 2023; Khorrami et al., 2023a; Yin et al., 2023; Youssefi et al., 2025). The fluctuations in the TWS are intrinsically connected to the changes occurring within its various compartments. Additionally, precipitation (P) and evapotranspiration (ET) are the key factors influencing the hydrological cycle, which in turn play a predominant role in the variations seen in both regional and global water cycles, ultimately affecting the dynamics of water storage and its availability (Rodell and Famiglietti, 2001). The natural and human-related forces impact the spatio-temporal dispersion of these hydroclimatic parameters, thus affecting the distribution of water storage (Khorrami et al., 2023b). Consequently, a thorough and accurate understanding of the dynamics of water storage and its availability requires an in-depth quantitative assessment of the variability in hydroclimatic factors that influence water storage fluctuations (Chao et al., 2023).

The Middle East (ME) experiences intense spatial variability in P, with the highest P (reaching over 1000 mm) falling across the coastal area. Overall, the precipitation rate in the region is very low, and the climatic conditions often result in evaporation rates that surpass the amount of precipitation (Evans et al., 2004). The ME predominantly experiences arid to semi-arid conditions, making fresh water a rare and valuable commodity. The interplay between limited freshwater availability and swift population growth significantly heightens the region's susceptibility to the impacts of future climate change. Since 1998, the area has undergone a series of droughts that have significantly affected its water resources (Khaki and Hoteit, 2021). Over recent decades, the surge in population and the escalating demand for food, energy, and water have significantly strained the environmental and water resources of the region. The situation has been further aggravated by the profligate consumption of water, particularly for irrigation purposes, which has significantly augmented over the last few decades in the pursuit of economic development (Alborzi et al., 2018). Consequently, a reduction in water storage, such as that caused by groundwater extraction, has been documented in multiple areas throughout the region (Haddadin, 2002). The depletion of groundwater and surface water resources across the ME poses a severe threat to human well-being, food security, and economic stability (Famiglietti, 2014). Because most countries in the region are developing nations with high population densities and limited adaptive capacity, continued water loss exacerbates existing socio-economic inequalities and undermines sustainable development. The water and groundwater decline that would inevitably threaten human survival and exacerbate regional development imbalance would be inevitable, as the ME is composed of developing countries with relatively denser populations and less advanced economies.

Over the past decade, GRACE/GRACE-FO has been widely applied across the Middle East to quantify TWS trends, groundwater depletion, drought, and downscaling approaches. Recent regional assessments report persistent storage decline over the Middle East and evaluate groundwater sustainability using GRACE/GRACE-FO and auxiliary data (e.g., Khaki and Hoteit, 2021). Country- and basin-level studies have expanded spatiotemporal analyses and methods, including comprehensive GRACE/GRACE-FO assessments for Iran (Amiri et al., 2023) and machine-learning downscaling/ensemble projections for Saudi Arabia (Yassin et al., 2024). Some researchers established substantial groundwater losses in the Tigris–Euphrates–western Iran region and broader Middle East and North Africa (MENA) using GRACE (e.g., Longuevergne et al., 2013; Voss et al., 2013). At national scales, recent investigations in the Arabian Peninsula and the UAE corroborate pronounced groundwater depletion and explore recharge diagnostics using GRACE with in-situ/model data (e.g., Alghafli et al., 2023). Collectively, this body of work documents persistent groundwater-dominated TWS declines across arid/semi-arid Middle Eastern settings and motivates our region-wide analysis linking GRACE/GRACE-FO storage changes with hydroclimatic drivers.

The existing literature indicates that several researchers have endeavored to illuminate the impact of various parameters on the fluctuations of TWS across multiple scales. These studies include Humphrey et al. (2016) (contribution of precipitation and air temperature at a global scale), Syed et al. (2008); Mo et al. (2016); Zhang et al. (2019) (contribution of P, ET and runoff at global scale), Pokhrel et al. (2021) (contribution of soil moisture at global scale), Felfelani et al. (2017) (contribution of snow water at global scale), Chao et al. (2023) (contributions of hydroclimatic components in the Yellow River Basin in China), and Aliabad and Ghaderpour (2025) (contribution of soil heat flux and soil temperature). The contribution of hydroclimatic parameters to water storage changes and variations in the available water may vary based on the geographical location (Chao et al., 2023) and the climatic conditions of the specific area under consideration. As a result, hydroclimatic variables exhibit varying influences on the fluctuations of TWS and its spatiotemporal variability across regions characterized by distinct climatic conditions.

Wavelet-based methods, particularly wavelet coherence, have been increasingly used to analyze hydroclimatic variability in the Middle East. For example, Rezaee et al. (2024) used wavelet transform to assess climatic dynamics and water availability in Iran (1961–2020); Araghi et al. (2017) used wavelet coherence to examine the relationship between three major climatic teleconnections and precipitation in Iran (1960–2014); Mallick et al. (2025) used GRACE-based groundwater storage anomalies and wavelet coherence to model groundwater drought and its teleconnections with global climate drivers in arid regions of Saudi Arabia (2002−2023) and Vaheddoost and Mohammadi (2025) investigated the relationship between GRACE-based TWS and 25 large-scale climate oscillation indices across 12 continental and subcontinental regions, applying correlation, principal component analysis, and wavelet-coherence methods to identify multi-scale teleconnections and significant spectral coherencies. These applications confirm the suitability of wavelet-based methods for capturing the multi-scale, non-stationary dynamics of water resources in arid and semi-arid environments, supporting their use in the present study.

The existing literature suggests that although several studies have examined groundwater and precipitation trends in parts of the Middle East, a comprehensive spatiotemporal analysis of TWS and WA, together with hydroclimatic contributions for the entire region, has not been carried out. Present research provides an elaborate analysis of the regional dynamics of water storage and water availability within the ME, while also quantifying the contribution of various hydroclimatic factors, including soil moisture, snow water, canopy water, groundwater, Precipitation (P), and Evapotranspiration (ET), in shaping the spatiotemporal dynamics of water storage utilizing component contribution ratio and wavelet coherence analysis approaches. The main contributions of the present work are as follows:

I. Trend analysis of TWS and WA, and the hydroclimatic variables across the ME at the pixel level and estimating the trends for the 18 countries in the ME since 2002.
II. Demonstrating the seasonal dynamics of TWS and WA and their driving hydroclimatic variables since 2002 for the ME.

III. Estimating the coherency and phase delays between the cycles of TWS, WA, and hydroclimatic variables for the largest countries with high populations in the ME, i.e., Iran, Turkey, Pakistan, Egypt, and Saudi Arabia.
IV. Estimating the contribution of hydroclimatic variables to TWS and WA dynamics over the ME and for the 18 countries in the ME since 2002.
V. Mapping the general climate condition of the ME.
VI. Estimating the contribution of hydroclimatic parameters to TWS in each climate zone.

The present research enhances the existing body of literature by elucidating the effects of changes in aridity on the extent of these contributions in the region, thereby addressing a notable gap in current research. A concise comparison of the previous regional studies against the current study is presented in Table 1.

2. Materials and methods

2.1. Study area

The ME (Fig. 1) is the world's driest region (Huang et al., 2016), where the annual precipitation is below the global mean (Khaki and Hoteit, 2021; Krishnamurti et al., 2024). The mean annual precipitation of the region reaches 1891 mm, while the ET shows a maximum value of 911 mm (Fig. 1). The region faces significant environmental challenges, with water scarcity being the most pressing issue that jeopardizes the future of the region (Khaki and Hoteit, 2021). The ME, which spans more than 7 million square kilometers, is inhabited by over 4.4 % of the world's population, living in diverse geographical environments that include coastal regions, mountainous terrains, and arid deserts (Shaban, 2022). The scarcity of water in the region has brought about an unequal distribution of this water resource across various geographical areas, resulting in environmental issues and geopolitical conflicts among countries that rely on shared water sources within the region (Shaban, 2022). A considerable portion of the ME is situated within the hyper-arid and arid zones (see Fig. 1b), highlighting the chronic insufficiency of water resources to meet the diverse demands for municipal, recreational, and industrial activities; for irrigation and aquaculture in agricultural contexts; as well as for non-consumptive applications, primarily in energy production and transportation (Haddadin, 2002).

This analysis involved the selection of 18 Middle Eastern countries, which were identified for their analogous arid to semi-arid hydroclimatic conditions and the water scarcity challenges they face. The national boundaries of these countries align with current socioeconomic indicators, population data, and policy measures, thereby increasing the relevance of the findings for decision-making and international water governance. The region is recognized as a geostrategically vital transboundary hydrological context, where country-level statistics play a crucial role in diplomacy and conflict resolution concerning shared water resources.

2.2. GRACE and GRACE-FO data

The Gravity Recovery and Climate Experiment (GRACE) represents a pioneering remote sensing project overseen by the National Aeronautics and Space Administration (NASA) of the United States and the German Space Agency (DLR). This mission entails the deployment of two satellites that orbit in tandem to gather data on the Earth's gravitational field (Tapley et al., 2019). The initiative began with the deployment of the first group of satellites in March 2002. The first GRACE mission (2002–2017) consisted of two satellites, flying in tandem in nearly identical orbits and continuously monitoring their inter-satellite range, range rate, and accelerations. This mission was succeeded in 2018 by the GRACE Follow-On (GRACE-FO) mission, which continues the long-term observation of Earth's time-variable gravity field. In this study, the TWS from the latest release (CSR mascon RL-06) of the GRACE/GRACE-FO datasets (with the spatial resolution of 25 km) was assessed to estimate the water storage dynamics over the ME from April 2002 to April 2024. A spatially continuous approach, using a gridded analysis, was adopted in the present study. Each grid cell was analyzed, and country-level results were obtained by area-weighted aggregation of the pixels that fall within each national boundary. This approach ensures full spatial coverage rather than random or purposive sampling, eliminating sampling bias.

Table 1
A summary of studies done on the ME with their main findings and limitations.

Ref.	Region	Data	Methods	Main Findings	Limitations
Voss et al. (2013)	Tigris–Euphrates	GRACE, GLDAS, Altimetry Data	GRACE mass change analysis; water balance decomposition; trend analysis	Significant GWS decline; unsustainable extraction	Limited to early GRACE record; uncertainties in separating TWS components; limited groundwater data
Khaki and Hoteit (2021)	Middle East	GRACE, GLDAS, Data Assimilation	Data assimilation; joint trend and drought analyses	Regional water storage loss; assimilation improved signal over arid regions	No WA–hydroclimate coupling; assimilation uncertainty; model dependence
Hussain et al. (2021)	Pakistan (Gilgit-Baltistan region)	GRACE Level 2 monthly data from CSR, GFZ, JPL; GLDAS-Noah; precipitation data	Least-squares regression; Spearman's rank correlations	Declining trends in TWS; Higher annual amplitude in GLDAS-Noah than GRACE	Trends were not statistically significant; coarse spatial resolution of GRACE in mountainous region
Amiri et al. (2023)	Iran (local scale)	GRACE-FO, GLDAS, climate reanalysis	GWS estimation from GRACE; trend analysis; correlation with quality indicators	Persistent TWS loss; validated GRACE trends with in-situ chemistry	No contribution ratio or climate stratification; discrepancy between GRACE signals and local well data
Yassin et al. (2024)	Saudi Arabia	GRACE-FO, in-situ water quality data, groundwater wells	Multi-step-ahead ML; forecasting experiments	ML ensemble methods show improvements; risks for long-term sustainability	Insufficient data for ML training; interpretability challenges; forecast uncertainty
Nikraftar et al. (2024)	Middle East	GRACE, ERA5, ML-ready data	Analytical groundwater sustainability index; trend and correlation analyses	59.14 % of the ME is unsustainable; presented sustainability metrics for policymakers	Focused only on GWS; no WA analysis; limited ground validation; assumptions impacting the accuracy of sustainability index
Present Study	Middle East (18 countries)	GRACE/GRACE-FO, GLDAS-Noah, CHIRPS, Aridity Index	CCR, STL, and LSCWA for trend, coherency and phase delay analyses	Quantified TWS, WA, and hydroclimatic drivers and studied their coherency and phase delays; open data	Reliance on the Noah LSM; uncertainties in harmonization of datasets and estimated trends

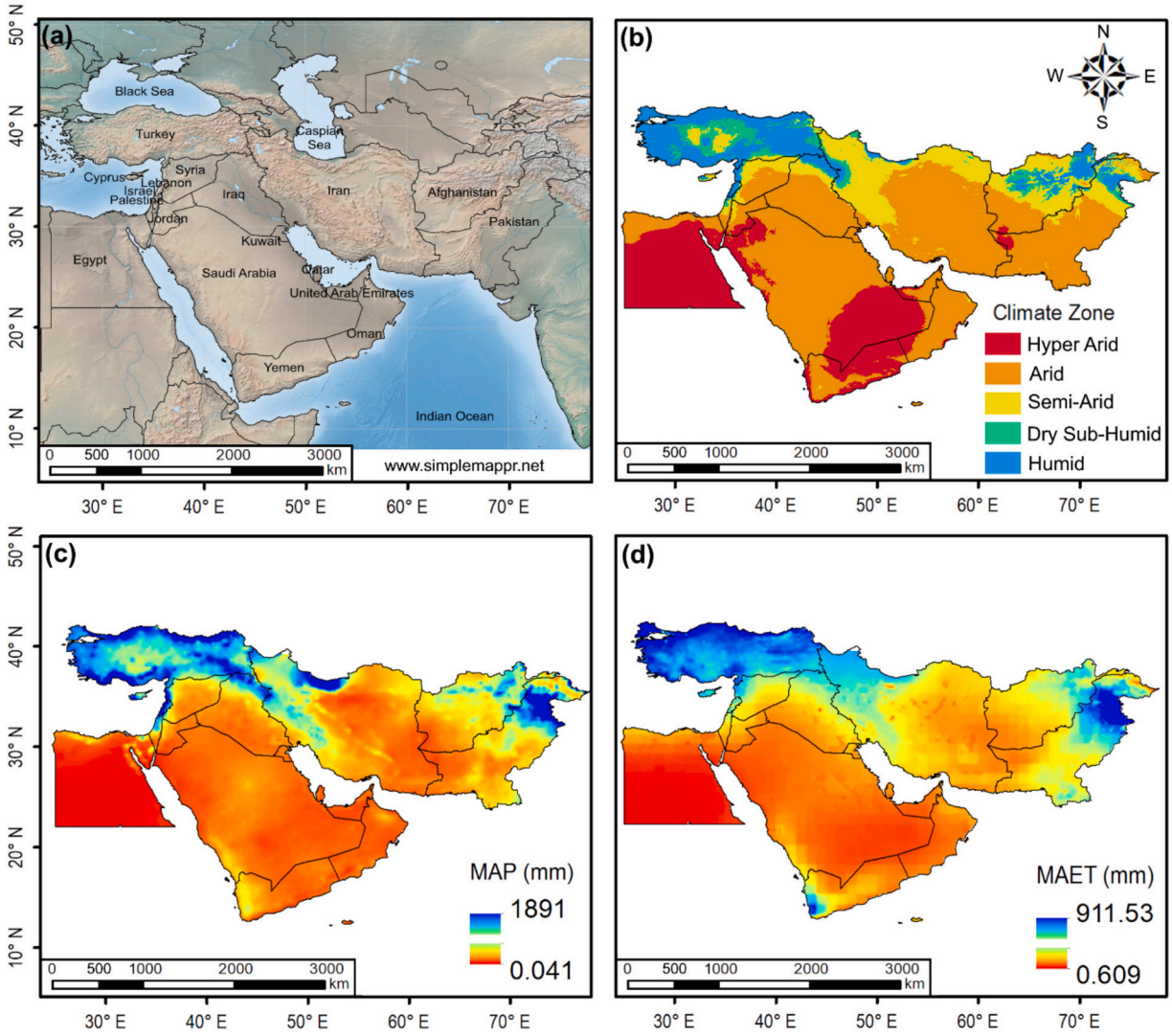

Fig. 1. (a) Geographic location of the Middle East, (b) Generic climate of the region based on aridity index, (c) Mean Annual Precipitation (MAP) map, and (d) Mean Annual Evapotranspiration (MAET) map.

2.3. GLDAS simulations

The Global Land Data Assimilation System (GLDAS) functions as a widely utilized comprehensive land surface model. Users can access the GLDAS dataset via five distinct land surface models, which include the Community Land Model (CLM), the Variable Infiltration Capacity (VIC) model, the Noah model, the Mosaic model, and the Catchment Land Surface Model (CLSM) (Rodell et al., 2004). The monthly values of Evapotranspiration (ET), Snow Water Equivalent (SWE), Soil Moisture Storage (SMS), and Canopy Water Storage (CWS) of the ME region were received from the Noah model at https://ldas.gsfc.nasa.gov/gldas/gldas-get-data (Last accessed on November 16, 2025). The Noah products demonstrated a higher degree of quality of match to GRACE TWSA than the other models (Wang et al., 2023). This analysis utilized the GLDAS Noah model data. The Noah model does not simulate Groundwater Storage (GWS). Instead, GWS was derived from the GRACE TWS by subtracting the hydrological components, such as SWE, CWS, and SMS.

2.4. CHIRPS data

The Climate Hazards Group InfraRed Precipitation with Station data (CHIRPS), a high-resolution (0.05 × 0.05 degrees) global precipitation dataset, is recognized for its high level of accuracy (Khorrami et al., 2024) and thus is frequently utilized as a substitute for precipitation measurements in areas where adequate data is lacking (Paca et al., 2020). The CHIRPS monthly precipitation data can be downloaded from https://www.chc.ucsb.edu/data/chirps (Last accessed on November 16, 2025).

To ensure consistency across datasets with varying native spatial resolutions (CHIRPS 0.05°, GLDAS Noah 0.25°, Global Aridity Index ~1 km, and GRACE mascon 0.25°), all products were spatially resampled to the GRACE resolution of 0.25° × 0.25° using bilinear interpolation (Chao et al., 2018; Ajjur and Al-Ghamdi, 2021). This harmonization allowed for direct comparison and integration of hydroclimatic variables. While resampling inevitably reduces the representation of local-scale heterogeneity, the focus of this study is on regional-to-country-level patterns. Therefore, the aggregated framework is appropriate and robust for the intended objectives.

2.5. Reconstruction of the missing GRACE /GRACE-FO data

The sporadic absence of TWS derived from the GRACE, along with an uninterrupted 11-month gap between GRACE and GRACE-FO, hinders the enhanced monitoring of water resources. Hence, it is imperative to fill in the missing months in the dataset. In this study, the missing months of the GRACE and GRACE-FO data were reconstructed using the

Seasonal and Trend decomposition using Loess (STL) proposed by Khorrami et al. (2023c). As a robust filtering technique for decomposing time-series datasets, the STL is employed to depict and define the actual TWS features observed by GRACE, encompassing both natural and human-induced influences. Consequently, it effectively fills in the missing information in the global TWS dataset (Khorrami et al., 2023c; Youssefi et al., 2025). The STL initially breaks down the time series data into its constituent parts, Eq. (1). Subsequently, it fills in the missing data by incorporating the mean seasonal and residual values, in addition to the trend component specific to the missing month, Eq. (2):

$$TWS_t = Trend_t + Seasonal_t + Residual_t \quad (1)$$

$$TWS_t = y\,(Trend_t) + \overline{Seasonal_t + Residual_t} \quad (2)$$

where $Trend_t$, $Seasonal_t$, $Residual_t$ at time t denotes the trend, seasonal, and residual of the TWS time series, respectively (Boergens et al., 2024). Eq. (2) estimates the missing value at time t by taking the estimated trend at time t and adding the mean of the seasonal plus residual components from other observed times (Ali et al., 2023). In the present study, there were 33 missing data points from the GRACE and GRACE-FO missions, including 22 months of mission gaps (20 gaps for the GRACE and two gaps for the GRACE-FO) as well as 11 months of intermission gaps (between the two missions). These gaps were closed using the STL technique to come up with a seamless dataset for the analysis.

2.6. Calculation of water availability and water storage changes

Water availability (WA) refers to the equilibrium between P and ET as the central water input and output variables of the hydrological cycle (Byrne and O'Gorman, 2015). Variations in water availability play a crucial role in the provision of freshwater resources, the assurance of food *sec*urity, and the maintenance of natural ecosystems, especially in regions characterized by limited water resources, where the growth of vegetation is predominantly influenced by the availability of water (Zhao et al., 2021). To estimate the WA of the ME region, P and ET values were derived from the Noah model and CHIRPS dataset from 2002 to 2024.

From the perspective of water balance, it is indicated that fluctuations in terrestrial water storage change (TWSC) are predominantly influenced by variations in P and ET (Yang et al., 2021), thus a close association between TWSC and WA is expected. The water balance methodology is typically employed to ascertain changes in water storage at both basin and continental levels, often serving as a reference point for other data products (Zhong et al., 2020). The TWSC is derived from the temporal derivative of TWS obtained from GRACE satellite data (Khorrami et al., 2023d). Monthly storage changes are determined by the difference between TWS values of two consecutive months at the start of a given month by Eq. (3):

$$TWSC = \frac{ds}{dt} = \frac{TWS_{t+1} - TWS_t}{\Delta t} \quad (3)$$

2.7. Component contribution ratio

The Component Contribution Ratio (CCR), as described by Kim et al. (2009), was used to estimate the contribution of different hydroclimatic parameters to the variations of water storage and water availability in the ME. In this premise, the contribution of (1) P and ET to Water Availability, (2) individual water storage components (including SWE, CWS, SMS, and GWS) to TWS, were estimated using Eqs. (4) and (5):

$$MAD_i = \frac{1}{N}\sum_{k=1}^{N} |S_{i_k} - \overline{S}_i| \quad (4)$$

$$CCR_i = \frac{MAD_i}{\sum_{j=1}^{n} MAD_j} \quad (5)$$

where MAD_i is the mean absolute deviation of the individual component S_i, N is the total number of components, $\overline{S}_i$ is the mean of each component S_i.

2.8. Aridity index

Aridity is generally characterized as a multifaceted function that integrates factors such as precipitation, temperature, and reference evapotranspiration. The Aridity Index (AI) is the ratio of potential evapotranspiration to precipitation, i.e., and determines the climatic conditions (Yang et al., 2019). In this research, the climatic condition of the ME was classified based on the AI of the region that was derived from the Global Aridity Index (Global-AI) datasets, specifically version 3, which operates at a resolution of 30 arc sec, or roughly 1 km at the equator. For additional details regarding the data and to access the download, please see the work of Zomer et al. (2022). According to AI values, the generalized climate is classified into five types: (i) Hyper Arid (AI <0.03), (ii) Arid ($0.03 \leq$ AI <0.2), (iii) Semi-Arid ($0.2 \leq$ AI <0.5), (iv) Dry Sub-humid ($0.5 \leq$ AI <0.65), and (v) Humid (AI ≥ 0.65).

2.9. Coherency and phase delay analysis

The least-squares cross wavelet analysis (LSCWA) serves as an effective analytical tool for examining the interrelationship between two time series across both temporal and spectral domains, enabling the assessment of coherency and phase delay (Ghaderpour and Pagiatakis, 2019). The LSCWA computes a time-frequency spectrogram for each time series using an effective windowing strategy. This tool can directly analyze time series which may have missing data and different sampling rates without any need for interpolation and/or time alignment. The LSCWA can consider the observational uncertainties and can estimate a higher time-frequency resolution cross-spectrogram compared to the traditional models, such as cross-wavelet transform (Grinsted et al., 2004; Ghaderpour, 2021). The LSCWA has been applied in many studies to investigate the interconnection between vegetation and hydroclimatic variables (Ghaderpour et al., 2021, Ghaderpour et al., 2023).

To estimate a spectrogram, a window whose size is inversely proportional to frequency translates over time and frequency. The sinusoids and trend constituents of known forms are simultaneously fitted to the segments within each translating (sliding) window. For a given set of frequencies, a spectrogram for each time series will be estimated, and then the two spectrograms (set to have the same dimensions) will be cross-multiplied. In LSCWA, within each window, the phases of the sinusoids are also estimated in order to calculate the phase differences, usually shown by arrows on the cross-spectrogram (LSCWS). Considering the normality of the residual series, a stochastic surface is also estimated in LSCWA to identify the peaks that are statistically significant at a certain confidence level, e.g., 95 %. The default settings of LSCWA are used in the present research, i.e., using 6 cycles of sinusoids and Gaussian weights (acting like Morlet wavelet) within translating windows. The default settings include a Gaussian window scale of c = 0.0125 with a window size allowing six sinusoidal cycles at a given frequency, as also suggested by Foster (1996) and Torrence and Compo (1998). These settings are proven to produce optimal time-frequency resolution spectrograms (Ghaderpour and Pagiatakis, 2017, 2019; Ghaderpour et al., 2021).

2.10. Mann-Kendall trend analysis

The Mann-Kendall (MK) trend test was employed to identify trends within the time series data. This non-parametric statistical method does not impose any assumptions regarding the distribution of the input

variables, making it a popular choice for examining trends in hydro-meteorological variables over time (Khorrami et al., 2023a; Khan and Li, 2025). Within the framework of the MK test, the null hypothesis (H_0) is formulated under the assumption that there is no underlying trend present in the time series. The assessment of each time series trend's significance was conducted at a significance level (α) of 0.05. The flowchart of this reseach is given in Fig. 2.

3. Results

3.1. Estimation of water storage and its fluctuations

To assess the fluctuations of TWS change in the ME, the TWS and its compartments, including SWE, CWS, SMS, and GWS, were used. The GWS variable was isolated from the column-integrated GRACE-observed TWS and the Noah simulations of SWE, CWS, and SMS. The time-series graph illustrating the long-term fluctuations of the TWS observed by GRACE, along with its four compartments across the ME (Fig. 3), was constructed utilizing the region-averaged values for each variable. The results demonstrate a wax and wane pattern for all the variables over the region, with a sharp diminishing trend for the TWS (− 0.048 cm/month) and GWS (− 0.049 cm/month) from April 2002 to April 2024. The analysis reveals that the SWE and the CWS exhibit no discernible trends; however, the SMS appears to be on the rise in the region, with a rate of 0.0016 cm/month. Furthermore, the results of the trend test suggest that there is no statistically significant trend detected in SMS, SWE, and CWS throughout the region.

For the spatial assessment of water storage fluctuations in the region, the long-term trends are illustrated in Fig. 4. From this figure, the variations of SWE and CWS are almost trivial in the region. This phenomenon can be attributed to the regional climate, which results in sparse vegetation and minimal snowpack for water retention. Notably, the SWE variations reveal significant reductions primarily in the northeastern parts of Turkey, Afghanistan, and Pakistan, where high mountain ranges are situated. The trend map of TWS and GWS shows almost identical changes through time, with the most critical situation in Iran for which the variations of TWS and GWS reach up to −4.55 cm/year and −4.73 cm/year, respectively. The circumstances are similarly dire in certain regions of Turkey, Iraq, Saudi Arabia, Afghanistan, and Pakistan. The observed spatial distribution of GWS fluctuations aligns closely with the results reported by Nikraftar et al. (2024). The variations in SMS indicate a downward trend across the central and northern parts of the region, particularly affecting Iran, Turkey, Iraq, and Syria.

The complete trend test results for each country are given in Table 2. The findings indicate that, with the exception of Yemen, where no notable trend is observed, the TWS has experienced a significant decline over the past two decades. The overall evaluation of the trends indicates that the ME region has experienced a severe loss of water storage during the study period which accounts for about −45 km^3/year equivalent to −1041 km^3 of total storage loss for the whole GRACE era. Iran appears to possess the most significant water storage condition among the countries in the Middle East, exhibiting a rate of −1.09 cm/year in TWS which is equivalent to about − 16.93 km^3/year and total water storage loss of − 389.37 km^3. Analyzing annual water storage depletion reveals that, following Iran, the countries experiencing the most significant losses from 2002 to 2024 are Jordan (−0.82 cm/year), Syria (−0.71 cm/year), Iraq (−0.66 cm/year), Afghanistan (−0.66 cm/year), Saudi Arabia (−0.64 cm/year), and Turkey (−0.56 cm/year). The alarming status of water storage variations in Iran, Syria, Iraq, Jordan, and Turkey was also documented from 2002 to 2015 (Bozorg-Haddad et al., 2020).

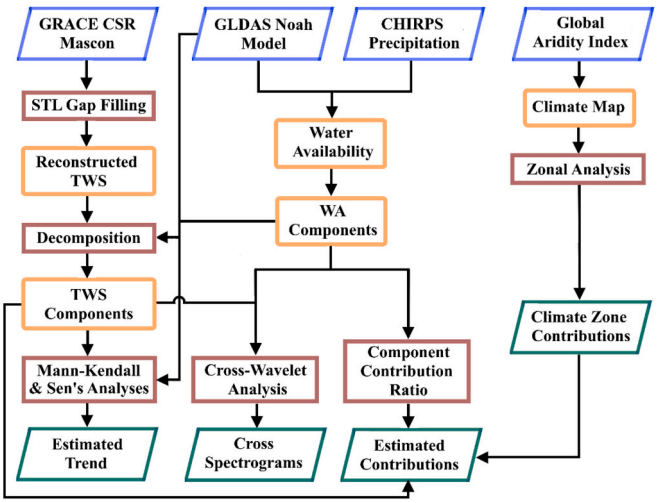

Fig. 2. Schematic Flow of the Analysis.

3.2. Changes in water availability

To delve into the spatio-temporal variations in water availability in the ME, the region-averaged values of P, ET, and WA are depicted in Fig. 5. The multi-year variations of WA and its components suggest that it follows the P variations in the region with a robust correlation of 0.74. The relationship between WA and ET in the region exhibits a moderate correlation of − 0.4. Given that P and ET are the primary factors influencing changes in Earth's water storage (Yang et al., 2021), a comparative analysis was conducted between the variations in WA and the changes in TWS derived from GRACE data (TWSC), the differential of two consecutive months of TWSA at the beginning of a month (Khorrami et al., 2023d), to explore the connections between water availability and fluctuations in water storage (Fig. 6). It shows that the long-term fluctuations of WA in the region are highly correlated (0.71) with the TWSC.

The mean monthly variations of WA in the region (Fig. 7) indicate that in the ME region, water availability varies from −3.70 cm to +14.06 cm per month. It reveals that the majority of Iran, Iraq, Syria, Egypt, Yemen, and Pakistan are crippled with water stress. The map also indicates that about half (49.46%) of the ME is under water stress with a negative WA value. These are the parts in the ME with low precipitation rates. Moreover, groundwater extraction for agricultural purposes in large irrigation areas like Pakistan, Central Turkey, and Iran leads to a substantial water deficit (Khaki and Hoteit, 2021). The northern parts of the region, in particular the coastal parts of Turkey, excluding central Anatolia, north of Iran, and Syria, west of Iraq, and north-east of Pakistan, show a high amount of WA. These areas are among the parts of the ME where P (30 cm/year) is above the regional average (10 cm/year) (Al-Taani et al., 2021; Khaki and Hoteit, 2021).

3.3. Seasonal dynamics of water storage and water availability

To check the seasonal dynamics of the parameters, the variations of TWS and WA, along with their drivers, extracted for each month of the study period. Fig. 8 portrays the temporal seasonal cycle of the parameters over the ME from April 2002 to April 2024. It is found that the TWS and GWS show decreasing values throughout all the seasons over the region. The minimum and maximum storage depletion values for the TWS occur in April (− 0.41 cm), and October (− 6.79 cm) respectively. While GWS shows the minimum and maximum variations in April (− 2.42 cm), and November (− 5.21 cm) respectively. The SWE increases from Jan to April and decreases throughout the remaining months over the region. The CWS shows no significant seasonal variations in the ME (Syed et al., 2008). The seasonal cycle of the SMS is increasing from January to May and decreasing through the remaining months. The maximum value of the SMS occurs in March (+ 1.94 cm), while it loses most of its storage in October (− 1.78 cm).

The seasonal dynamic of the WA and its drivers shows that the region

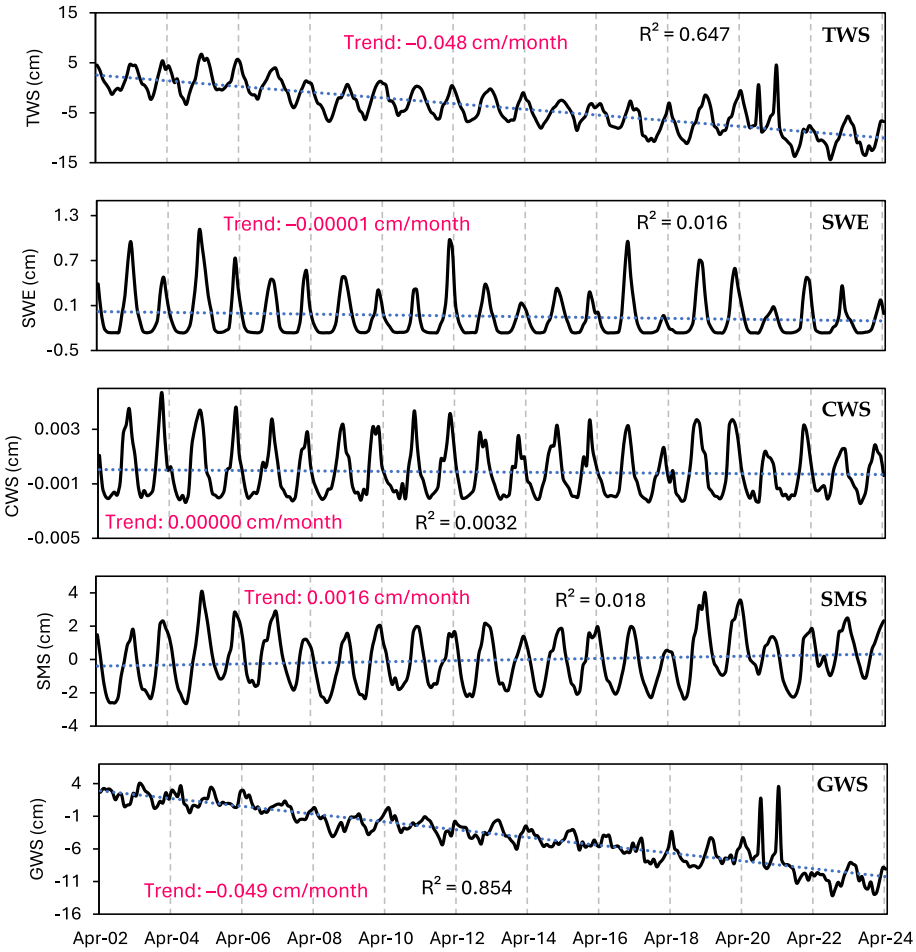

Fig. 3. Region-averaged fluctuations of TWS and its compartments over the ME.

receives the highest volume of water through P in April (2.90 cm), while it reaches the lowest value in December (0.68 cm). The seasonality of P in April aligns well with the seasonality of TWS and GWS when the maximum P corresponds to the minimum loss of water and groundwater storage in the region. On the other hand, ET demonstrates varying patterns with the minimum and maximum variations in January (0.75 cm) and July (2.79 cm), respectively. The WA seasonality indicates that the region experiences positive WA values (increased water availability) from January to Jun, while from July to December the region suffers from water stress. The maximum values of WA are in April (+1.62 cm), which concurs with the seasonal dynamics of TWS, GWS, and P in the region, indicating that the increasing P and water storage lead to surplus water availability in the ME. The region suffers from the least available water in September, with a minimum WA of − 1.21 cm.

Seasonality can also epitomize the variability within a year. This research employed standard deviation as a method to compute and illustrate the seasonal variations of hydroclimatic parameters throughout the year (Wasko et al., 2020). The standard deviation serves to quantify the extent of variability among members of a group. An increased standard deviation indicates a higher level of variability within a specific year, suggesting a more significant seasonal impact. Conversely, a decreased standard deviation reflects a lower degree of seasonal variability.

The seasonality maps (Fig. 9) demonstrate the spatial patterns of the seasonal cycle for TWS, WA, and their components over the region. According to the result, TWS and GWS have similar seasonal patterns where the most seasonal impacts are observed over northern and southern Iran, Turkey, north of Saudi Arabia, and east of Afghanistan and Pakistan. The ME region experiences the maximum seasonality of TWS and GWS, reaching up to 34.50 cm and 36.90 cm, respectively. SWE shows its maximum seasonality (15 cm) over eastern Turkey and some parts of north-east Pakistan and east of Afghanistan. Notwithstanding its trivial seasonality, CWS also demonstrates the same pattern over the region. SMS, with similar seasonal patterns, has the maximum seasonality (12.32 cm) mainly over Turkey.

Ragrading the seasonality of WA, and its components, it is understood from the maps that there is an overall spatial overlap between the seasonal patterns of WA, P, and ET. ET shows seasonal dynamic patterns identical to those of SMS, with the most variations in Turkey, which reveals the direct association between soil moisture and ET. P suffers from the most seasonal impacts mainly in the coastal areas of Turkey, the west, and north-west of Iran, and partly over east of Afghanistan, and Pakistan. With the same spatial dispersion, the seasonal value of WA reaches its maximum value (14.67 cm) over the coastal areas of Turkey, the west, and north-west of Iran. Overall, it is safe to state that the seasonality pattern of WA and its components mimics that of the TWS and its compartments over the ME, indicating that seasonal variations of hydroclimatic parameters in the ME conspicuously affect the variability of water storage and water availability.

3.4. LSCWA results

In the present study, LSCWA is applied to time series of TWS, WA, and their respective components for five counties in the ME that have the largest size and populations, i.e., Iran, Turkey, Pakistan, Egypt, and Saudi Arabia. The LSCWA results are illustrated in Figs. 10 and 11 and Figs. S1-S8. The small white arrows in these figures indicate the relative phases present between the time series. The orientation of the arrows

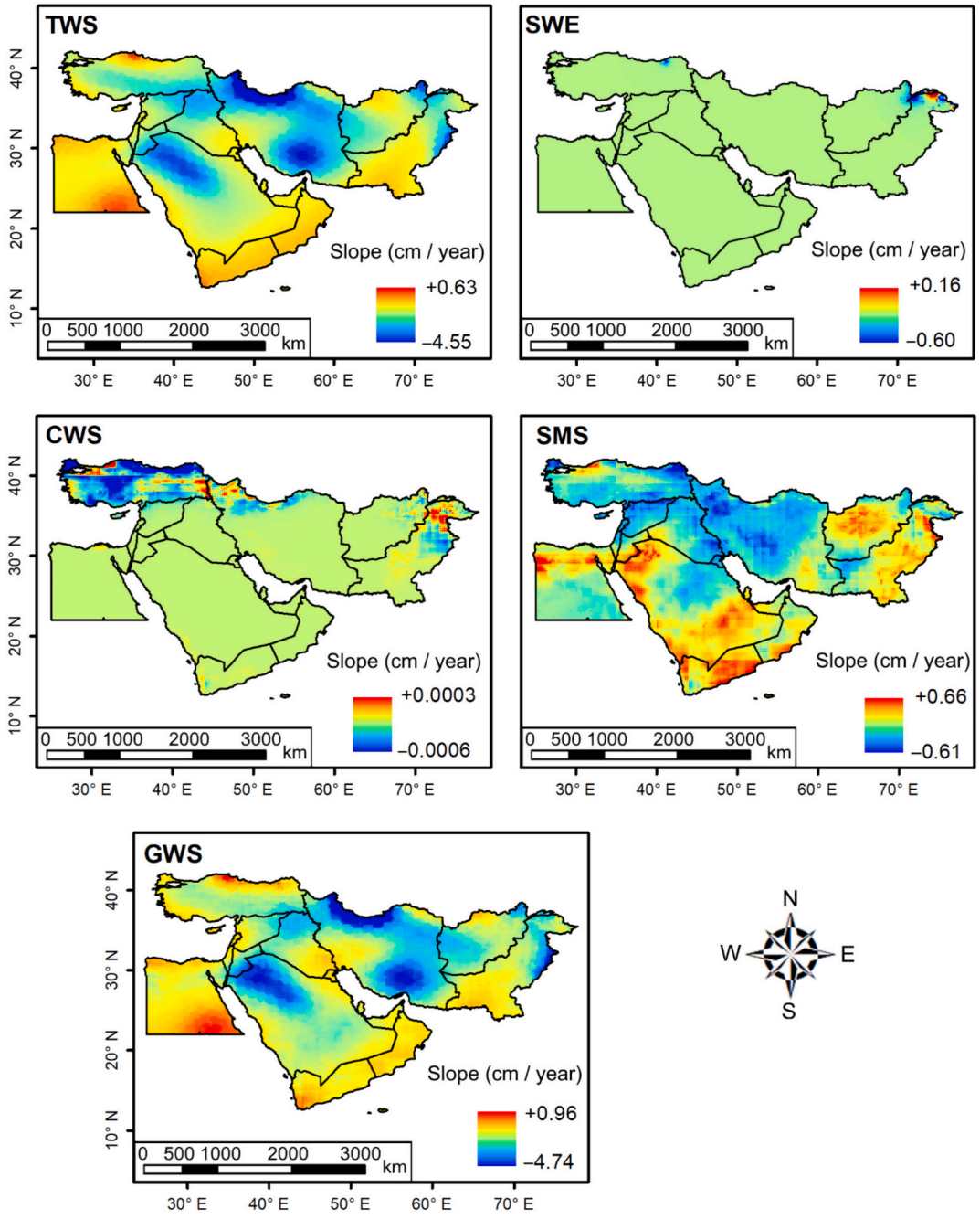

Fig. 4. Multi-year trend of fluctuations of TWS and its compartments over the ME.

pointing from left to right signifies in-phase alignment, whereas the arrow directed from right to left denotes anti-phase alignment. The upward vertical arrow represents a lag of 90 degrees in the second time series relative to the first time series, while the downward vertical arrow indicates a lag of 90 degrees in the first time series relative to the second time series. The spectral peaks that are statistically significant at a 95 % confidence interval are also within the back contour lines. Note that the cross-spectrograms are obtained after simultaneous fitting and removing linear trends within translating windows as described in Ghaderpour et al. (2021, 2023).

From Fig. 10, the annual cycles of the time series are the most dominant peaks. Approximately 80 % annual coherency is observed between 2010 and 2015 between TWS and its components CWS, SMS, and GWS, while the annual coherency significantly reduced after 2020. The annual cycles of TWS generally lag behind the annual cycles of SWE, CWS, and SMS by approximately two to three months, while they lead the annual cycles of GWS by approximately two months. Fig. 10 shows that the GWS has the most intense associations with the fluctuations of TWS, particularly before 2015. From Fig. 11 and Figs. S2 and S6, the annual cycles of WA, P, and ET are the most dominant cycles in Iran, Turkey, and Egypt, while in Pakistan (Fig. S4), the semi-annual cycles and in Saudi Arabia (Fig. S8), 3 cycles/year (four-month period) are the most dominant cycles. Fig. 11 also shows that the annual cycles of precipitation time series generally lead the ones in the WA time series by a couple of months, while the annual cycles of ET lag the ones in WA by about a month and, in some periods, are in phase. Similarly, for Turkey (Fig. S2) and Egypt (Fig. S6).

Table 2
Trend of the country-wide fluctuations of TWS (April 2002 – April 2024).

Country Name	TWS Trend			*P*-value	Trend test ($\alpha = 0.05$)
	cm/yr	km^3/yr	Total loss (km^3)		
Iran	−1.09	−16.93	−389.37	0.000	*descending trend
Saudi Arabia	−0.64	−11.96	−274.99	0.000	*descending trend
Turkey	−0.55	−4.65	−107.05	0.000	*descending trend
Afghanistan	−0.66	−4.13	−95.06	0.000	*descending trend
Pakistan	−0.36	−2.94	−67.59	0.000	*descending trend
Iraq	−0.66	−2.77	−63.66	0.000	*descending trend
Syria	−0.71	−1.31	−30.11	0.000	*descending trend
Yemen	−0.32	−1.14	−26.27	0.070	No trend
Jordan	−0.82	−0.70	−16.03	0.000	*descending trend
Egypt	−0.05	−0.45	−10.34	0.016	*descending trend
Oman	−0.07	−0.18	−4.24	0.000	*descending trend
United Arab Emirates	−0.28	−0.17	−3.94	0.000	*descending trend
Israel	−0.43	−0.09	−1.98	0.000	*descending trend
Kuwait	−0.24	−0.04	−0.93	0.000	*descending trend
Lebanon	−0.26	−0.03	−0.61	0.000	*descending trend
Qatar	−0.25	−0.02	−0.54	0.000	*descending trend
Cyprus	−0.24	−0.02	−0.41	0.000	*descending trend
Palestine	−0.23	−0.01	−0.33	0.000	*descending trend

(*) denotes that the test results are significant.

3.5. Contribution of hydroclimatic parameters

Based on the CCR analysis, the contributions of hydroclimatic parameters to the fluctuations of TWS and WA in the ME were quantified. The spatial illustration of the results is given in Fig. 12. The findings reveal that CWS contributes the least to the TWS variations with a maximum value of 0.0004 %. Although its contribution is seen to cover mainly central and eastern Turkey, western Iran, and Afghanistan, its value is too low to be safely neglected. The area-averaged contribution values (Table 3) indicate that CWS has no contribution to the TWS of ME countries. The spatial map of SWE suggests that it is more effective on the variations of TWS in eastern Turkey, north-east of Pakistan, and Afghanistan, with a maximum contribution ratio of 58%. The country-averaged values show that among the ME countries, only 5 countries: Turkey (4.90%), Afghanistan (4.50%), Pakistan (3.71%), Iran (0.36%), and Lebanon (0.01%) benefit from SWE variations. For the remaining parts of the ME, SWE has no role in the variations of water storage. On the other hand, SMS turns out to be a very determining parameter controlling the variations of TWS in the ME, with the maximum contribution ratio of 81.5%. SMS manifests the most contribution to the TWS variations in Lebanon (60.22%), Cyprus (53.12%), Kuwait (552.05%), and Turkey (48%). It is less effective in Egypt, with a contribution of 9.26%. The strongest contributor to the variations of TWS in the region is GWS, with the spatial contribution ratio ranging from 18.5% to 99.90%. GWS controls the water storage of the majority of the ME, particularly Egypt, Jordan, Saudi Arabia, the United Arab Emirates, and Iran, with a mean contribution ratio of more than 80%. From a visual perspective, it can be stated that GWS contributes mainly to those areas where SMS has the least contribution to the TWS and vice versa.

It should be noted that GWS is not directly simulated by GLDAS Noah and was therefore derived as the residual of GRACE TWS after removing SWE, CWS, and SMS. This residual definition means that GWS will, by construction, account for a substantial fraction of TWS variability, particularly in arid and semi-arid regions where snow and canopy water contributions are minor. Therefore, the contribution of GWS identified here should be interpreted as reflecting the dominance of residual storage in the GRACE signal rather than as an entirely independent component.

The contribution of P and ET to the variations of WA is also given. It is found that although P and ET both contribute considerably to WA in the ME, P, with the maximum spatial contribution ratio of 90.40%, has relatively more domination compared to ET. P and ET show complementary contributions to the variations of WA. To put it another way, the contribution of P is higher over part of the region where ET has the lowest impact, and vice versa. For instance, while P shows the most contribution to the variations of WA in Lebanon (74.26%), ET has the least contribution in this country, with a ratio of 25.74%. Similarly, ET is the strongest contributor to WA in Egypt with a ratio of 71.98%, whereas P has the least contribution of 28.02%.

3.6. Mapping the general climate condition of the ME

To evaluate the contribution ratio of hydroclimatic parameters over different aridity levels in the ME, the generalized classification scheme for Aridity Index (AI) values was used to map the variations of aridity over the ME (Fig. 13).

The spatial variations in the AI over the region suggest that from May to October, the majority of the ME is under hyper-arid conditions due to increased aridity. According to the resulting aridity map of the region (Fig. 1b), it is found that about half (49.02%) of the region falls in the Arid climate type. The second dominant climate type of the region is a Hyper-arid climate covering about 19.95% of the ME. The remaining parts of the region experience the general climate type of semi-arid (14.98%), humid (10.84%), and dry sub-humid (5.22%). Overall, it

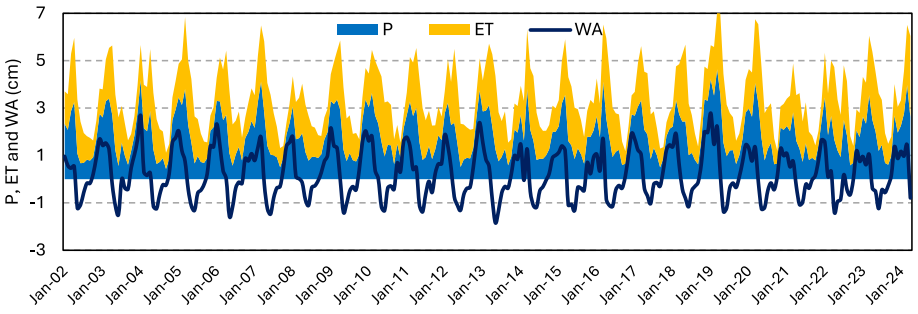

Fig. 5. Temporal fluctuations of P, ET, and WA over the ME.

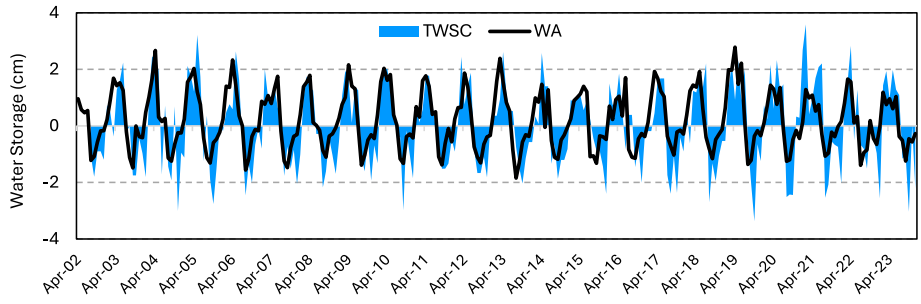

Fig. 6. Temporal associations between WA and TWSC over the ME.

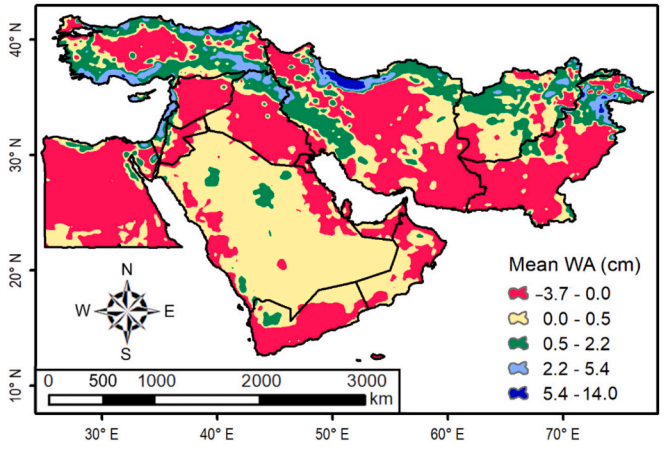

Fig. 7. Mean monthly variations of WA over the ME (April 2002 – April 2024).

can be concluded that about 84% of the ME region is under pressure from aridity.

3.7. Changes in contribution magnitude in response to aridity

To evaluate the contribution of each Hydroclimatic variable to the fluctuations of water storage and water availability in response to the variations in aridity, the contribution of the parameters was extracted across different climate categories identified for the region (Fig. 1b). According to the results (Table 4), CWS has no role in the variations of TWS. SWE is ineffective under hyper-arid conditions, while it shows the highest contribution (7.45%) to TWS variations in humid areas. SMS also manifests its highest magnitude of contribution (44.27%) in humid parts, while it is the least effective under hyperarid conditions with a contribution ratio of 12.59%. The ascendancy of GWS is seen under a hyper-arid climate, where it contributes to about 87.41% of the TWS variations. At its heaviest magnitude, GWS contributes to about 48.28% of the TWS of areas with humid areas.

The results also indicate that P has the most influence on the variations of WA of the region, with a contribution of 62.89% in areas under dry sub-humid conditions. It is the least effective parameter in hyper-arid conditions, with a contribution ratio of 40.37%. ET turns out to be the most effective parameter (59.63%) of WA variations in hyper-arid climates, while in humid areas it has the least contribution (37.85%). Overall, taking the wanes and waxes of the parameter contribution rates, it is inferred that the contribution of SWE, SMS, and GWS follows exactly the variations of climate type. SMS and SWE contribution values increase as the general climate of the region gets wetter (from hyper-arid to humid). A contrary situation is seen for GWS, where its influence weakens as the climate gets wet. For the P and ET, there is no stable increasing or decreasing pattern with changes in aridity.

4. Discussion

4.1. Variations in water storage and water availability

The spatial patterns of TWS fluctuations in the ME are consistent with global and regional assessments (Mo et al., 2016; Scanlon et al., 2016; Bozorg-Haddad et al., 2020; Khaki and Hoteit, 2021), indicating the reliability of the findings. The GRACE observations reveal that the majority of the ME region has a negative trend of water storage variations (Bozorg-Haddad et al., 2020; Khaki and Hoteit, 2021), indicating that during the GRACE era (April 2002–April 2024), the water storage of the region has been depleting, resulting in a huge volume of storage loss. This indicates a very critical situation for the countries in the region, especially the top seven countries (such as Iran, Jordan, Syria, Iraq, Afghanistan, Saudi Arabia, and Turkey) with the most significant water storage loss during the same period. The critical status of water storage shrinkage in these countries was also reported by Khaki and Hoteit

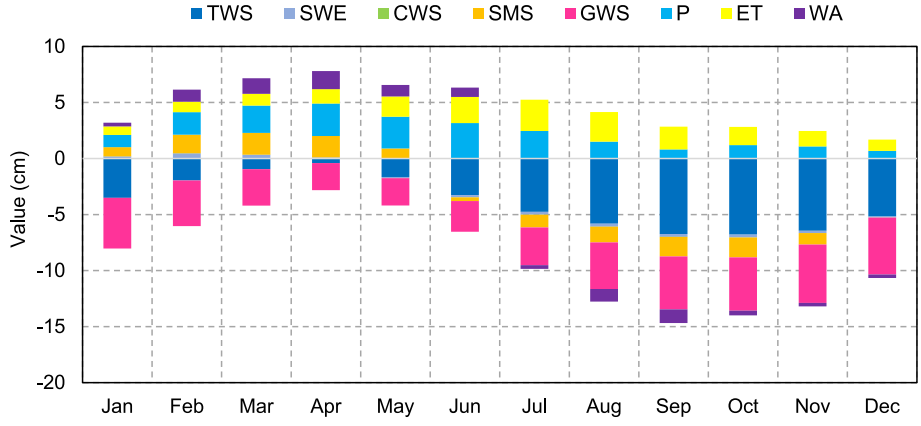

Fig. 8. Seasonal dynamics of TWS, WA, and their compartments (2002–2024).

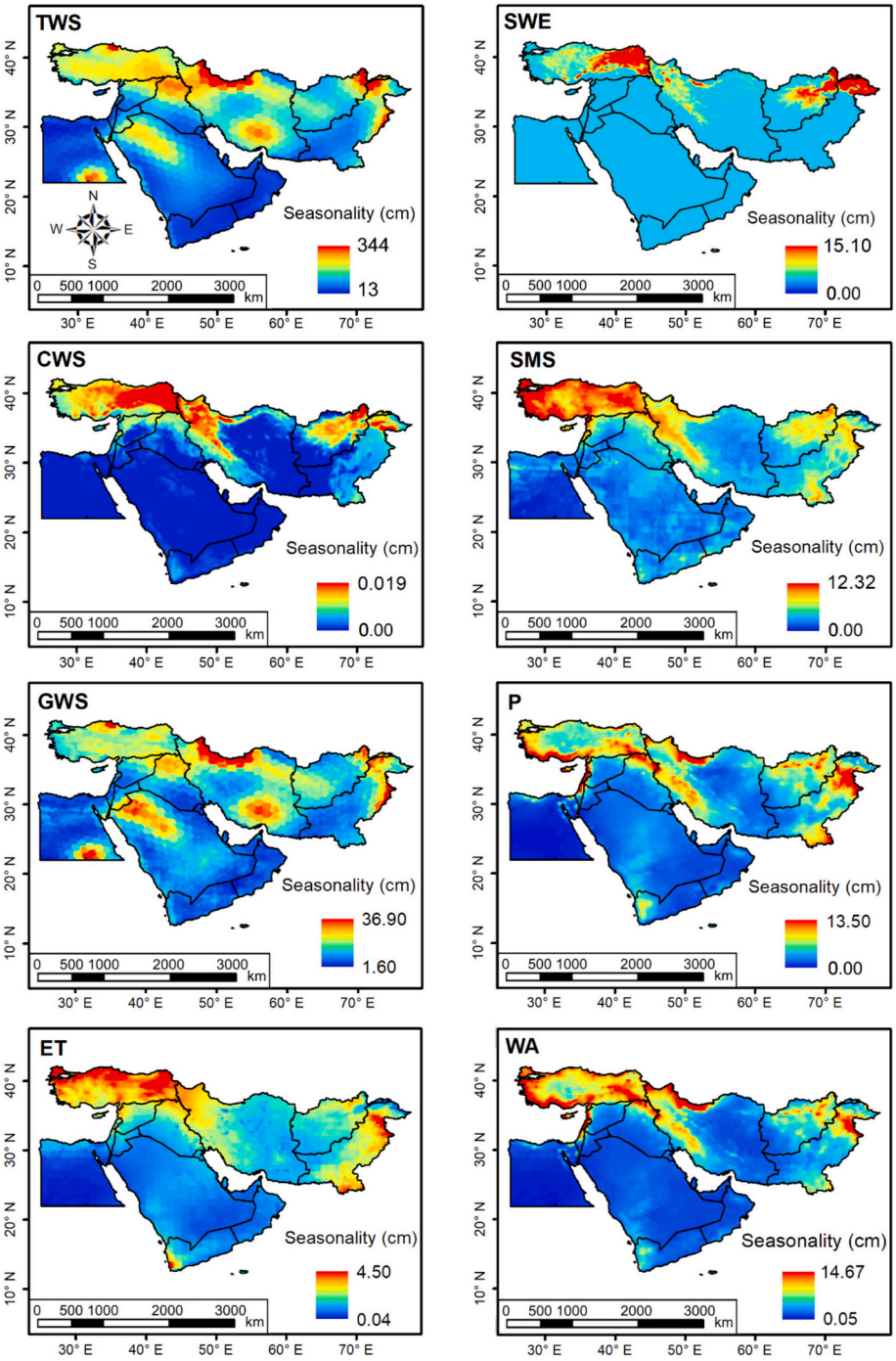

Fig. 9. Seasonality of TWS, WA, and their drivers over the ME (2002–2024).

(2021).

Fluctuations of groundwater also show a pattern similar to that of the TWS in the region. The findings suggest considerable depletion in Iran, Türkiye, Iraq, Saudi Arabia, Afghanistan, as well as east of Pakistan. Notably, considerable GWS depletion was also reported for Iran, Turkey, and Afghanistan during 1980–2019 (Khaki and Hoteit, 2021). The harsh water storage decline in these areas of the ME is ascribed, to a great degree, to the pernicious impacts of prolonged droughts and a lesser degree, the water use by domestic and industry sectors (Khaki and Hoteit, 2021). According to the literature, the ME region has gone through mega-droughts in 1998–2001 and 2007–2008 largely due to La Niña effects (Barlow et al., 2016). Severe drought incidents during the years between 2000 and 2020 were identified and reported in Iran (Hameed et al., 2018; Lashkari et al., 2021), Turkey (Khorrami and Gunduz, 2021), Iraq (Hameed et al., 2018), Saudi Arabia (Syed et al., 2022), Afghanistan (Rousta et al., 2020), and Pakistan (Ali et al., 2021, 2022).

The study also finds that CWS has no variations in the ME region, which is mainly associated with the dominant dry situation in the region. Notwithstanding their spatial variations, SWE and SMS show an insignificant trend over the region. A decreasing trend of SMS is seen in the center and north of the region, mainly over Iran, Turkey, Iraq, and Syria. The same situation in Turkey and Iran was also reported by Khaki and Hoteit (2021). They ascribed the diminishing SMS of these countries to the changes in precipitation and stream flow.

The surface water storage (SWS) component was neglected in the

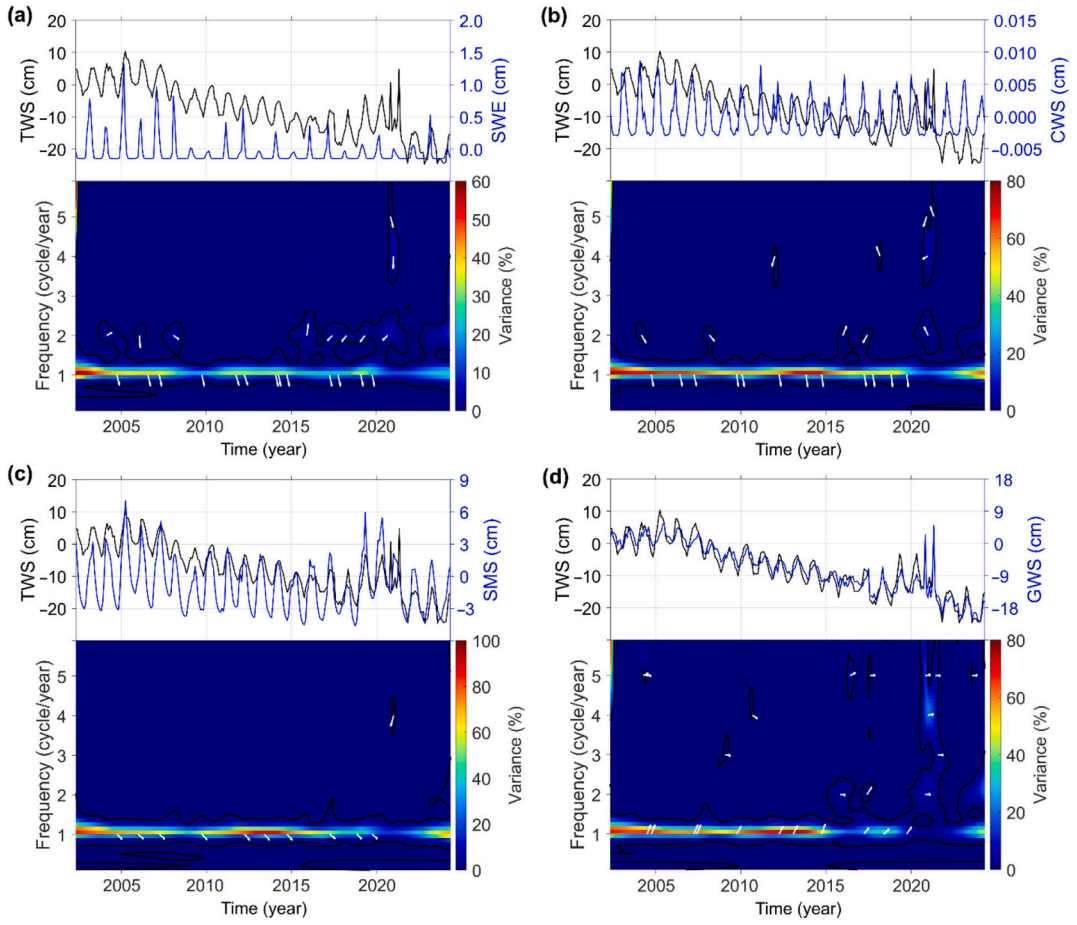

Fig. 10. LSCWSs between TWS and (a) SWE, (b) CWS, (c) SMS, and (d) GWS time series for Iran. The arrows show the phase delays. Arrows pointing to the right, left, up, and down mean the cycles of the two time-series are in phase, out of phase, TWS leads, and TWS lags, respectively. The spectral peaks inside the black contour lines are statistically significant at a 95 % confidence level.

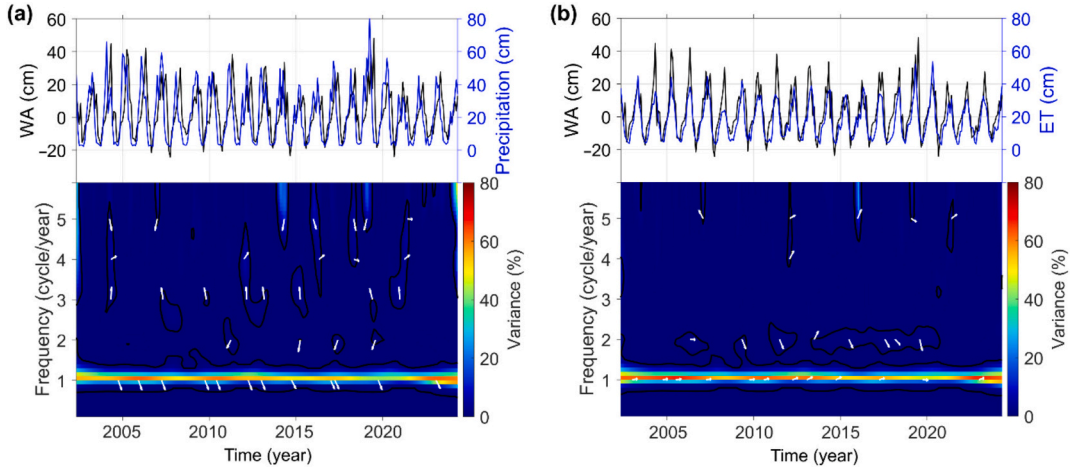

Fig. 11. LSCWSs between WA and (a) precipitation, and (b) ET time series for Iran, see the caption of Fig. 10 for more details.

analysis of water storage variations in this study. Although the WaterGAP model simulates SWS of the world, this study did not use those simulations mainly due to their incompatible spatial and temporal resolution with the data used in this study. Moreover, excluding the tropical regions of the world, the impact of the variations of surface water is typically minimal relative to that of the remaining compartments (SMS, GWS, and SWE) (Rodell and Famiglietti, 2001; Zhang et al., 2024).

The WA analysis indicates that the majority of the region is under water stress with a negative WA on average. Although water scarcity detected in Iran, Iraq, Syria, Egypt, Yemen, and Pakistan aligns well with the variations in TWS and GWS over these areas, overall, there seems not to be a harmonic relationship between WA and TWS on a spatial domain. This is probably due to the nature of the GRACE estimates. While WA reflects the pure impacts of climatic variations (in P and ET) on water

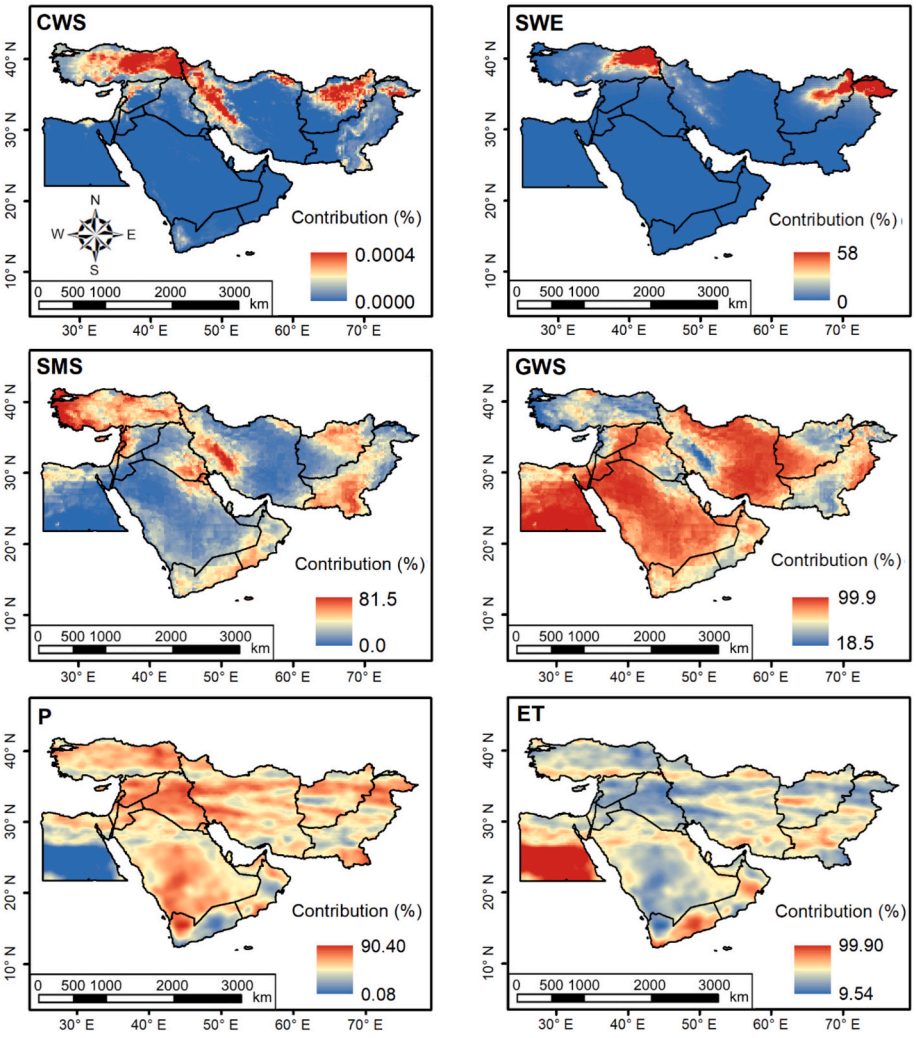

Fig. 12. Spatial illustration of contribution of hydroclimatic parameters to TWS and WA variations over the ME.

Table 3
Contribution ratio of hydroclimatic parameters to TWS and WA.

Country Name	Contribution to TWS (%)				Contribution to WA (%)	
	SWE	CWS	SMS	GWS	P	ET
Iran	0.36	0.00	18.40	81.23	59.65	40.35
Saudi Arabia	0.00	0.00	12.95	87.05	60.27	39.73
Turkey	4.90	0.00	48.0	47.10	60.89	39.11
Afghanistan	4.50	0.00	26.10	69.40	59.45	40.55
Pakistan	3.71	0.00	32.62	63.67	57.05	42.95
Iraq	0.03	0.00	25.67	74.30	71.17	28.83
Syria	0.00	0.00	27.48	72.52	69.87	30.13
Yemen	0.00	0.00	30.80	69.20	48.87	51.13
Jordan	0.00	0.00	11.08	88.92	66.75	33.25
Egypt	0.00	0.00	9.26	90.74	28.02	71.98
Oman	0.00	0.00	32.29	67.71	52.65	47.35
United Arab Emirates	0.00	0.00	18.41	81.59	57.28	42.72
Israel	0.00	0.00	24.79	75.21	60.98	39.02
Kuwait	0.00	0.00	52.05	47.95	63.66	36.34
Lebanon	0.01	0.00	60.22	39.77	74.26	25.74
Qatar	0.00	0.00	22.51	77.49	51.19	48.81
Cyprus	0.00	0.00	53.12	46.88	67.04	32.96
Palestine	0.00	0.00	40.41	59.59	64.74	35.26

availability, the GRACE senses both the climatic and anthropogenic signals; therefore, the GRACE-observed TWS epitomizes both climatic- and human-induced variations (Jing et al., 2020). The side effects of human intervention on water resources in the ME region have already been reported by multiple studies (Joodaki et al., 2014; Khaki et al., 2018; Haghighi and Motagh, 2019; Khaki and Hoteit, 2021). The mean monthly variation map of WA of the ME (Fig. 7) shows that the northern parts of the region (mainly coastal parts of Turkey, northern parts of Iran, and north of Syria and western Iraq), on average, benefit from more available water than other parts with more availability. This can be ascribed to the above-normal precipitation received in these areas. This finding agrees well with the findings of Khaki and Hoteit (2021).

4.2. *Parameters' contribution*

The analysis of parameter contribution to TWS over the ME reveals that GWS and SMS together are the cardinal controlling parameters of its water storage variations. GWS, with an average contribution ratio of 75.72% is the key contributor to the water storage fluctuations in the ME. This signals the large extent of GWS depletion in the region (Konikow and Kendy, 2005). This may be directly associated with the anthropogenic pressure on the water resources in arid regions (Joodaki et al., 2014; Scanlon et al., 2012a, 2012b), where the majority of water requirements are met through the extraction of groundwater from aquifers due to the limited water provided by precipitation. The finding that GWS contributes most to TWS variability in the Middle East must be interpreted with caution, since GWS is defined as a residual of GRACE TWS after removing smaller components. Consequently, its high

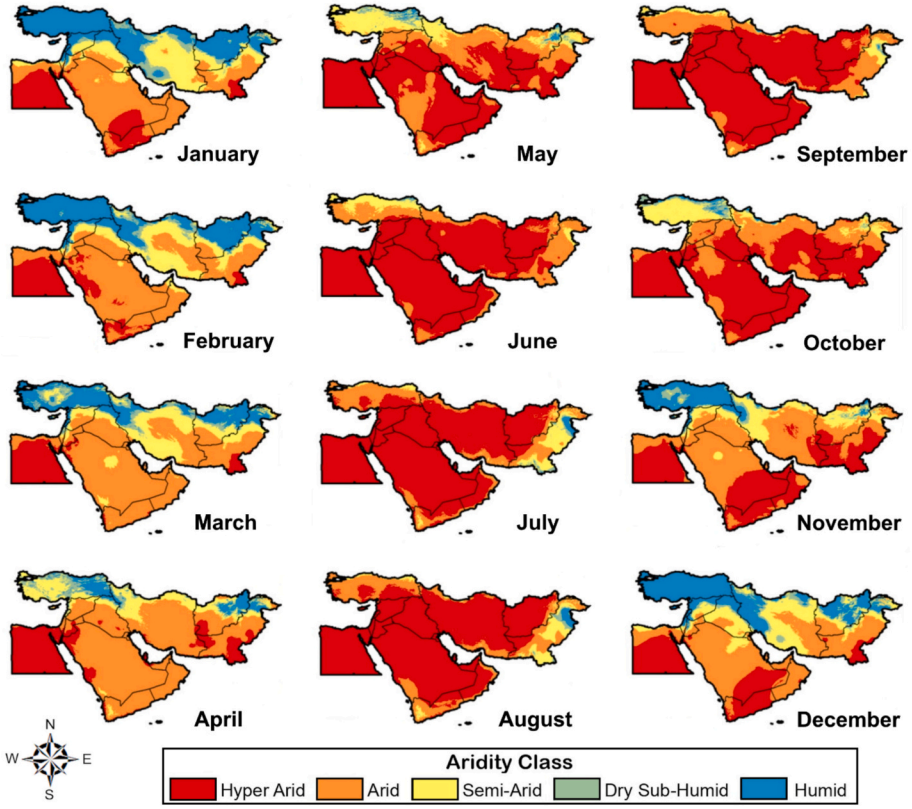

Fig. 13. Spatial illustration of seasonal variability of the aridity index over the Middle East.

Table 4
Contribution of Hydroclimatic Parameters to Water Storage in each climate zone.

	Parameters	Hyper-Arid	Arid	Semi-Arid	Dry Sub-Humid	Humid
CContribution to TWS	SWE	0.00%	0.18%	1.95%	4.54%	7.45%
	CWS	0.00%	0.00%	0.00%	0.00%	0.00%
	SMS	12.59%	20.14%	28.53%	37.79%	44.27%
	GWS	87.41%	79.69%	69.52%	57.66%	48.28%
Contribution to WA	P	40.37%	59.51%	61.98%	62.89%	62.15%
	ET	59.63%	40.49%	38.02%	37.11%	37.85%

contribution is expected by construction. Nevertheless, this pattern is consistent with hydrological conditions in the Middle East, where groundwater withdrawal and depletion dominate water storage changes (Döll et al., 2012; Scanlon et al., 2012a, 2012b; Joodaki et al., 2014; Khaki and Hoteit, 2021). Our results, therefore, reinforce existing evidence of GWS as the primary driver of regional water storage decline, rather than presenting an entirely independent discovery.

With a region-averaged contribution ratio of 22.97%, SMS is the second strongest contributor to TWS variations in the region. The country statistics suggest that SMS controls the TWS variations in Lebanon, Cyprus, Kuwait, and Turkey. The superior contribution of SMS to TWS fluctuations in Turkey is also reported by Khorrami and Gunduz (2021). The remaining 1.31% of the contribution belongs to SWE, which is chiefly effective in the mountainous regions of north-east Türkiye, west of Iran, east and north-east of Afghanistan, and Pakistan. The results indicate that, except in Egypt, for which WA is controlled by ET, for the remaining countries of the ME, it is P that contributes the most to the variations of WA (Zhang et al., 2019).

The dominance of GWS over SMS in arid and hyper-arid climates can be attributed to the fundamental water- and energy-balance constraints governing these regions. In arid regions, precipitation is extremely limited and transient; surface and soil moisture stores are small and have low buffering capacity. Consequently, much of the long-term water signal is stored or lost from deeper stores (groundwater). Pumping and long groundwater residence times mean that changes in groundwater are both large in magnitude and slow to recover, so they dominate the multi-year TWS variance detected by GRACE. Irrigation, urban extraction, and return-flow patterns in arid economies produce persistent declines in aquifer storage that are well captured by GRACE's low-frequency signal. Examples include Iran, Saudi Arabia, and parts of Iraq, where intensive pumping for agriculture has created large, long-term groundwater deficits.

SMS contributions exhibit a clear upward trend from hyper-arid (12.59 %) to humid climates (44.27 %), reflecting fundamental shifts in hydrological processes across the climate gradient. In humid regions, higher and more frequent precipitation events sustain soil moisture for longer periods, making the upper soil layers highly responsive to short-term hydroclimatic variability. The greater vegetation density in these climates further enhances root-zone water storage and intensifies soil–vegetation interactions, contributing to stronger soil moisture fluctuations that are detectable in GRACE-derived TWS anomalies. Additionally, well-developed soils in wetter climates possess higher infiltration capacities and greater retention potential, enabling them to store and release water more effectively than the shallow, crusted, and rapidly evaporating soils typical of hyper-arid regions. Together, these factors explain why SMS becomes progressively more influential in

controlling TWS variability toward humid climates, emphasizing the dominant role of shallow hydrological components in regulating water storage dynamics under wetter environmental conditions. Therefore, the CCR gradients across climate zones embody both natural hydroclimatic processes and human-induced pressures, providing a process-based interpretation that complements the descriptive spatial patterns identified in Section 3.7.

4.3. Eco-hydrological and socio-economic dimensions

The persistent depletion of water storage has far-reaching ecological, hydrological, and socio-economic implications. TWS anomalies can amplify land–atmosphere feedback, influencing climate extremes and ecosystem functioning (Levine et al., 2016; Xiong and Yang, 2025). Reduced groundwater storage jeopardize wetlands, riparian ecosystems, and biodiversity, including critical stopover sites for Palearctic migratory birds (Walther and Huettmann, 2021). Declining soil moisture and precipitation may accelerate desertification processes, disrupt vegetation phenology, increase soil temperature at depth, and impair ecosystem services, such as carbon sequestration and dust suppression (Aliabad et al., 2025).

Socio-economically, declining water storage threatens agricultural productivity, urban water supply, and regional food security. These effects may intensify rural–urban migration and cross-border displacement, amplifying humanitarian and security challenges (McLeman, 2022). When groundwater is insufficient to meet plantation water demand, or when competition arises between irrigation needs and other human uses of groundwater, plantations are likely to experience high mortality, rendering afforestation efforts unsustainable (Chen et al., 2018). The hydroclimatic shifts detected in this study are also embedded within broader telecoupled socio-ecological processes that transcend national boundaries. For example, persistent GWS depletion in the Tigris–Euphrates basin has been amplified by upstream dam construction and irrigation expansion in Turkey and western Iran, triggering downstream water deficits and agricultural losses in Iraq and Syria (Voss et al., 2013; Khaki and Hoteit, 2021). Similarly, intensive abstraction within the Arabian Peninsula aquifer systems supports irrigated agriculture and urban supply but at the cost of rapid groundwater mining and heightened energy demand for desalination and pumping (Muhammad et al., 2021). These cases exemplify telecoupling, where hydrological stress in one sub-region propagates through trade, migration, and virtual water flows to neighboring economies (Liu et al., 2013; Cattaneo et al., 2019). The resulting dependence on imported food and energy further links ME water scarcity to global markets, emphasizing that water management must be coordinated within the water–energy–food nexus. Incorporating such cross-scale interactions into adaptation planning and transboundary governance frameworks would strengthen the policy relevance of satellite-based hydroclimatic monitoring presented herein.

Moreover, the substantial water consumption required to sustain healthy plantations can negatively impact the eco-hydrology of adjacent ecosystems at both local and regional scales, particularly under conditions of excessive groundwater extraction (Cao et al., 2010; Sun and Vose, 2016). Local groundwater depletion can propagate to distant systems through global grain markets, energy trade, and migration corridors (Chen et al., 2018). For example, declining irrigation capacity in Iran and Iraq can elevate global food prices, while increasing reliance on virtual water imports, thus linking Middle Eastern water security to global supply chains.

These regional impacts resonate globally through telecoupling, the set of socio-environmental interactions across distances (Liu et al., 2013). Water scarcity in the Middle East manifests through several interconnected pathways. Reduced irrigation capacity intensifies dependence on food imports (Hakimian, 2003), altering agricultural patterns and agricultural trade under limited water conditions and culminating in shifts in imports/exports (Hejazi et al., 2023). Water-driven displacement further places demographic and economic pressure on neighboring countries, reshaping regional socio-political landscapes. Moreover, diminished river flows and wetland loss disrupt migratory bird routes (Donnelly et al., 2020), leading to cascading effects on species survival across Eurasia and Africa. Incorporating telecoupling into water resource assessments highlights how unsustainable groundwater exploitation in one country can generate far-reaching transboundary impacts. Collectively, these cross-scale linkages highlight that ME water scarcity is not an isolated regional challenge but part of a telecoupled water–energy–food–ecology system. Addressing these interconnected risks requires coordinated governance, transboundary cooperation, and integration of satellite-based hydroclimatic monitoring into regional water-policy frameworks.

4.4. Policy and management implications

The findings of the present study underscore the urgent need for integrated water-management frameworks across the ME, where declining terrestrial water storage and groundwater depletion threaten long-term sustainability. Strengthening transboundary water cooperation and data-sharing mechanisms is essential, particularly under the UN Economic and Social Commission for Western Asia (UN-ESCWA) regional water strategy. The observed groundwater-dominated storage loss highlights the importance of regulating agricultural abstraction and adopting Food and Agriculture Organization (FAO) Water Scarcity Initiative principles to enhance efficiency in irrigation and recharge management.

Moreover, the openly shared datasets and analytical framework developed in the current study can support regional decision-makers and stakeholders in developing evidence-based policies for climate adaptation, drought early warning, and sustainable groundwater allocation. By quantifying the climatic and anthropogenic contributions to water storage decline, this research provides a robust foundation for science-informed governance of scarce water resources in one of the world's driest regions.

4.5. Limitations and future directions

A limitation of this study is the harmonization of datasets with different native spatial resolutions to the GRACE mascon scale (0.25°). This step, while necessary for intercomparison, may reduce the representation of fine-scale heterogeneity and propagate uncertainty across scales. However, given the study's focus on regional-scale variability, we expect these effects to be minor for the main conclusions. Another limitation is the reliance on the Noah LSM alone for estimating non-groundwater components of TWS. While Noah has been shown to perform well in arid and semi-arid regions, including parts of the ME (Bulut et al., 2019; Amini et al., 2023), structural uncertainty remains. Future work should consider the use of multi-model ensembles (e.g., Noah, CLM, VIC, and Mosaic) to reduce this uncertainty and provide more robust estimates of groundwater storage changes. The third limitation is ascribed to the Mann–Kendall trend analysis for which no pre-whitening, variance correction, or multiple-testing adjustment was applied. Therefore, while the large regional and country-scale trends reported here are robust due to the strength of the GRACE signal, some country-level results may be sensitive to autocorrelation and multiple-comparison effects. Incorporating such corrections in future studies would provide more conservative estimates of significance. In this study, the Mann–Kendall trend analysis was applied alongside least-squares cross-wavelet analysis (LSCWA) to identify trends and measure coherency. However, it is well recognized that machine learning (ML) and hybrid artificial intelligence models present robust options for predictive modeling of TWS. Research utilizing Random Forest, Gradient Boosting, and long short-term memory (LSTM) networks has effectively captured the nonlinear interactions between climate drivers and groundwater storage (Wang et al., 2023). While this

methodology emphasizes interpretability and transparency, future research could incorporate ML-based hindcasting or explainable AI techniques (such as SHAP values) to yield causal insights and projections for the near future, thereby increasing the policy relevance of TWS evaluations.

5. Conclusions

This study assessed the spatiotemporal dynamics of terrestrial water storage and water availability in the Middle East using GRACE/GRACE-FO observations combined with hydrological model outputs and precipitation datasets. Several key insights emerge:

- **Groundwater dependence:** Groundwater is the dominant driver of TWS variability across most of the ME, underscoring the heavy reliance on aquifers and the urgent need for sustainable groundwater management in this arid to semi-arid region.
- **Widespread water scarcity:** Nearly half of the region consistently experiences negative WA, highlighting the structural imbalance between water supply and demand and the vulnerability of regional populations to climate variability and anthropogenic pressure.
- **Climatic modulation of contributions:** The role of different hydroclimatic variables varies with climate zones. In wetter zones, soil moisture and snow storage become more important, while in arid zones, groundwater overwhelmingly governs storage changes.
- **Policy and management relevance:** These findings provide scientific evidence to inform national and transboundary water management, particularly in regions where aquifer depletion is accelerating.

While the study provides a robust regional-scale assessment, some limitations remain. The residual definition of groundwater storage, the use of mixed-source datasets for P and ET, and the lack of explicit uncertainty propagation should be considered when interpreting results. Future work should integrate process-based hydrological models with GRACE to better constrain water balance closure and uncertainty.

The results of this study are essential for the understanding of the dynamics of water storage and water availability in the ME region. They can significantly improve our understanding of the factors influencing GRACE-observed TWS variations in the region and may assist researchers when dealing with GRACE disintegration practices. The authors also hold the notion that a more detailed and precise understanding of hydrological processes of water storage and availability in the region can be obtained through hydrological modeling, with one of the most effective options being an integrated model such as ParFlow-CLM (Maxwell and Miller, 2005) and TerrSysMP (Shrestha et al., 2014). By integrating physical processes, such as surface and subsurface flow, infiltration, and evapotranspiration, models provide robust insights into water dynamics across varying landscapes and time scales (Soltani et al., 2022, 2024). This approach would allow for a more accurate representation of water storage and availability in the ME, complementing the GLDAS dataset analysis.

CRediT authorship contribution statement

Fahimeh Youssefi: Writing – original draft, Visualization, Methodology, Formal analysis, Data curation, Conceptualization. **Behnam Khorrami:** Writing – original draft, Visualization, Methodology, Formal analysis, Data curation, Conceptualization. **Shoaib Ali:** Writing – review & editing, Formal analysis, Conceptualization. **Samira Sadat Soltani:** Writing – review & editing, Conceptualization. **Mohammad Javad Valadan Zoej:** Writing – review & editing, Supervision, Conceptualization. **Jonathan Li:** Writing – review & editing, Supervision, Conceptualization. **Ebrahim Ghaderpour:** Writing – original draft, Visualization, Supervision, Methodology, Formal analysis, Conceptualization.

Funding

This study was supported by Space It Up, funded by the Italian Space Agency (ASI) and the Ministry of University and Research (MUR), under contract n. 2024-5-E.0 CUP n. I53D24000060005.

Declaration of competing interest

The authors declare that they have no known competing financial interests or personal relationships that could have appeared to influence the work reported in this paper.

Appendix A. Supplementary data

Supplementary data to this article can be found online at https://doi.org/10.1016/j.ecoinf.2025.103571.

Data availability

The datasets used in this study are publicly available from the following sources:•

GRACE/GRACE-FO Mascon Solutions (CSR RL06): https://www2.csr.utexas.edu/grace/•

GLDAS Noah Model Data: https://ldas.gsfc.nasa.gov/gldas/gldas-get-data•

CHIRPS Precipitation Data: https://www.chc.ucsb.edu/data/chirps•

Global Aridity Index Dataset (v3): https://www.global-ai-pet.org/

All processed datasets (resampled GRACE/GRACE-FO TWSA, GLDAS Noah outputs, CHIRPS precipitation, derived GWS, WA) are available at Zenodo at: https://doi.org/10.5281/zenodo.17119514

The LSCWA code implemented in this study which comes with a Graphical User Interface (GUI) is available at: https://github.com/Ghaderpour/LSWAVE-SignalProcessing (see folder: MATLAB-Package_EGhaderpour with the main code: LSWAVE_GUI.m).

References

Ajjur, S.B., Al-Ghamdi, S.G., 2021. Evapotranspiration and water availability response to climate change in the Middle East and North Africa. Clim. Chang. 166, 28. https://doi.org/10.1007/s10584-021-03122-z.

Alborzi, A., Mirchi, A., Moftakhari, H., Mallakpour, I., Alian, S., Nazemi, A., AghaKouchak, A., 2018. Climate-informed environmental inflows to revive a drying lake facing meteorological and anthropogenic droughts. Environ. Res. Lett. 13, 084010. https://doi.org/10.1088/1748-9326/aad246.

Alghafli, K., Shi, X., Sloan, W., Shamsudduha, M., Tang, Q., Sefelnasr, A., Ebraheem, A. A., 2023. Groundwater recharge estimation using in-situ and GRACE observations in the eastern region of the United Arab Emirates. Sci. Total Environ. 867, 161489. https://doi.org/10.1016/j.scitotenv.2023.161489.

Ali, S., Liu, D., Fu, Q., Cheema, M.J.M., Pham, Q.B., Rahaman, M.M., Anh, D.T., 2021. Improving the resolution of GRACE data for spatio-temporal groundwater storage assessment. Remote Sens. 13, 3513. https://doi.org/10.3390/rs13173513.

Ali, S., Liu, D., Fu, Q., Cheema, M.J.M., Pal, S.C., Arshad, A., Pham, Q.B., Zhang, L., 2022. Constructing high-resolution groundwater drought at spatio-temporal scale using GRACE satellite data based on machine learning in the Indus Basin. J. Hydrol. 612, 128295. https://doi.org/10.1016/j.jhydrol.2022.128295.

Ali, S., Ran, J., Luan, Y., Khorrami, B., Xiao, Y., Tangdamrongsub, N., 2023. The GWR model-based regional downscaling of GRACE/GRACE-FO derived groundwater storage to investigate local-scale variations in the North China plain. Sci. Total Environ. 908, 168239. https://doi.org/10.1016/j.scitotenv.2023.168239.

Aliabad, F.A., Ghaderpour, E., 2025. Modeling soil heat flux from MODIS products for arid regions. Eco. Inform. 86, 103005. https://doi.org/10.1016/j.ecoinf.2025.103005.

Aliabad, F.A., Ghaderpour, E., Zare, M., Bozzano, F., 2025. A novel remote sensing approach for estimating soil temperature at depth. Eco. Inform. 91, 103432. https://doi.org/10.1016/j.ecoinf.2025.103432.

Al-Taani, A.A., Nazzal, Y., Howari, F.M., 2021. Groundwater scarcity in the Middle East. In: Global Groundwater. Elsevier, pp. 163–175. https://doi.org/10.1016/B978-0-12-818172-0.00012-8.

Amini, A., Karami Moghadam, M., Abdeh Kolahchi, A., Raheli-Namin, M., Ahmed, K.O., 2023. Evaluation of GLDAS soil moisture product over Kermanshah province, Iran. H2Open J. 6 (3), 373–386. https://doi.org/10.2166/h2oj.2023.057.

Amiri, V., Ali, S., Sohrabi, N., 2023. Estimating the spatio-temporal assessment of GRACE/GRACE-FO derived groundwater storage depletion and validation with in-

situ water quality data (Yazd province, Central Iran). J. Hydrol. 620, 129416. https://doi.org/10.1016/j.jhydrol.2023.129416.
Araghi, A., Mousavi-Baygi, M., Adamowski, J., Martinez, C., 2017. Association between three prominent climatic teleconnections and precipitation in Iran using wavelet coherence. Int. J. Climatol. 37 (6), 2809–2830. https://doi.org/10.1002/joc.4881.
Arij, N., Latifi, H., Fakhri, A., Esmaili, R., 2025. Four decades of spatio-temporal trends in Miankaleh wetland's water body and vegetation as revealed by remote sensing time series. Eco. Inform. 91, 103374. https://doi.org/10.1016/j.ecoinf.2025.103374.
Barlow, M., Zaitchik, B., Paz, S., Black, E., Evans, J., Hoell, A., 2016. A review of drought in the Middle East and Southwest Asia. J. Clim. 29, 8547–8574. https://doi.org/10.1175/JCLI-D-13-00692.1.
Boergens, E., Güntner, A., Sips, M., Schwatke, C., Dobslaw, H., 2024. Interannual variations of terrestrial water storage in the East African Rift region. Hydrol. Earth Syst. Sci. 28, 4733–4754. https://doi.org/10.5194/hess-28-4733-2024.
Bozorg-Haddad, O., Zolghadr-Asli, B., Sarzaeim, P., Aboutalebi, M., Chu, X., Loáiciga, H. A., 2020. Evaluation of water shortage crisis in the Middle East and possible remedies. J. Water Supply Res. Technol. AQUA 69, 85–98. https://doi.org/10.2166/aqua.2019.049.
Bulut, B., Yilmaz, M.T., Afshar, M.H., Şorman, A.Ü., Yücel, İ., Cosh, M.H., Şimşek, O., 2019. Evaluation of remotely-sensed and model-based soil moisture products according to different soil type, vegetation cover and climate regime using station-based observations over Turkey. Remote Sens. 11, 1875. https://doi.org/10.3390/rs11161875.
Byrne, M.P., O'Gorman, P.A., 2015. The response of precipitation minus evapotranspiration to climate warming: why the "wet-get-wetter, dry-get-drier" scaling does not hold over land. J. Clim. 28, 8078–8092. https://doi.org/10.1175/JCLI-D-15-0369.1.
Cao, S., Tian, T., Chen, L., Dong, X., Yu, X., Wang, G., 2010. Damage caused to the environment by reforestation policies in arid and semi-arid areas of China. Ambio 39 (4), 279–283. https://doi.org/10.1007/s13280-010-0038-z.
Cattaneo, C., Beine, M., Fröhlich, C.J., Kniveton, D., Martinez-Zarzoso, I., Mastrorillo, M., Millock, K., Piguet, E., Schraven, B., 2019. Human migration in the era of climate change. Review of Environmental Economics and Policy 13 (2), 189–206. https://doi.org/10.1093/reep/rez008.
Chao, N., Luo, Z., Wang, Z., Jin, T., 2018. Retrieving groundwater depletion and drought in the Tigris-Euphrates Basin between 2003 and 2015. Groundwater 56, 770–782. https://doi.org/10.1111/gwat.12611.
Chao, N., Li, F., Yu, N., Chen, G., Wang, Z., Ouyang, G., Yeh, P.J.F., 2023. Divergent spatiotemporal variability of terrestrial water storage and eight hydroclimatic components over three different scales of the Yangtze River basin. Sci. Total Environ. 879, 162886. https://doi.org/10.1016/j.scitotenv.2023.162886.
Chen, J., John, R., Sun, G., Fan, P., Henebry, G.M., Fernández-Giménez, M.E., Qi, J., 2018. Prospects for the sustainability of social-ecological systems (SES) on the Mongolian plateau: five critical issues. Environ. Res. Lett. 13, 123004. https://doi.org/10.1088/1748-9326/aaf27b.
Döll, P., Hoffmann-Dobrev, H., Portmann, F.T., Siebert, S., Eicker, A., Rodell, M., Strassberg, G., Scanlon, B.R., 2012. Impact of water withdrawals from groundwater and surface water on continental water storage variations. J. Geodyn. 59, 143–156. https://doi.org/10.1016/j.jog.2011.05.001.
Donnelly, J.P., King, S.L., Silverman, N.L., Collins, D.P., Carrera-Gonzalez, E.M., Lafón-Terrazas, A., Moore, J.N., 2020. Climate and human water use diminish wetland networks supporting continental waterbird migration. Glob. Chang. Biol. 26 (4), 2042–2059. https://doi.org/10.1111/gcb.15010.
Ershadfath, F., Shahnazari, A., Raeini Sarjaz, M., Andaryani, S., Trolle, D., Olesen, J.E., 2024. Blue and green water availability under climate change in arid and semi-arid regions. Eco. Inform. 82, 102743. https://doi.org/10.1016/j.ecoinf.2024.102743.
Evans, J.P., Smith, R.B., Oglesby, R.J., 2004. Middle East climate simulation and dominant precipitation processes. Int. J. Climatol. 24, 1671–1694. https://doi.org/10.1002/joc.1084.
Famiglietti, J.S., 2014. The global groundwater crisis. Nat. Clim. Chang. 4, 945–948. https://doi.org/10.1038/nclimate2425.
Felfelani, F., Wada, Y., Longuevergne, L., Pokhrel, Y.N., 2017. Natural and human-induced terrestrial water storage change: a global analysis using hydrological models and GRACE. J. Hydrol. 553, 105–118. https://doi.org/10.1016/j.jhydrol.2017.07.048.
Forootan, E., Rietbroek, R., Kusche, J., Sharifi, M.A., Awange, J.L., Schmidt, M., Famiglietti, J.S., 2014. Separation of large-scale water storage patterns over Iran using GRACE, altimetry and hydrological data. Remote Sens. Environ. 140, 580–595. https://doi.org/10.1016/j.rse.2013.09.025.
Foster, G., 1996. Wavelet for period analysis of unevenly sampled time series. Astron. J. 112, 1709–1729. https://doi.org/10.1086/118137.
Frappart, F., Ramillien, G., 2018. Monitoring groundwater storage changes using the gravity recovery and climate experiment (GRACE) satellite mission: a review. Remote Sens. 10, 829. https://doi.org/10.3390/rs10060829.
Ghaderpour, E., 2021. Least-squares wavelet and cross-wavelet analyses of VLBI baseline length and temperature time series: Fortaleza-Hartrao-Westford-Wettzell. Publ. Astron. Soc. Pac. 133, 1019. https://doi.org/10.1088/1538-3873/abcc4e.
Ghaderpour, E., Pagiatakis, S.D., 2017. Least-squares wavelet analysis of unequally spaced and non-stationary time series and its applications. Math. Geosci. 49, 819–844. https://doi.org/10.1007/s11004-017-9691-0.
Ghaderpour, E., Pagiatakis, S.D., 2019. LSWAVE: a MATLAB software for the least-squares wavelet and cross-wavelet analyses. GPS Solutions 23, 50. https://doi.org/10.1007/s10291-019-0841-3.
Ghaderpour, E., Vujadinovic, T., Hassan, Q.K., 2021. Application of the least-squares wavelet software in hydrology: Athabasca River basin. J. Hydrol. Reg. Stud. 36, 100847. https://doi.org/10.1016/j.ejrh.2021.100847.
Ghaderpour, E., Mazzanti, P., Scarascia Mugnozza, G., Bozzano, F., 2023. Coherency and phase delay analyses between land cover and climate across Italy via the least-squares wavelet software. Int. J. Appl. Earth Obs. Geoinf. 118, 103241. https://doi.org/10.1016/j.jag.2023.103241.
Grinsted, A., Moore, J.C., Jevrejeva, S., 2004. Application of the cross wavelet transform and wavelet coherence to geophysical time series. Nonlinear Process. Geophys. 11, 561–566. https://doi.org/10.5194/npg-11-561-2004.
Haddadin, M.J., 2002. Water issues in the Middle East challenges and opportunities. Water Policy 4, 205–222. https://doi.org/10.1016/S1366-7017(02)00028-4.
Haghighi, M.H., Motagh, M., 2019. Ground surface response to continuous compaction of aquifer system in Tehran, Iran: results from a long-term multi-sensor InSAR analysis. Remote Sens. Environ. 221, 534–550. https://doi.org/10.1016/j.rse.2018.11.003.
Hakimian, H., 2003. Water scarcity and food imports: an empirical investigation of the'virtual water'hypothesis in the MENA region. Rev. Middle East Econ. Financ. 1 (1), 71–85. https://doi.org/10.1080/1475368032000061653.
Hameed, M., Ahmadalipour, A., Moradkhani, H., 2018. Apprehensive drought characteristics over Iraq: results of a multidecadal spatiotemporal assessment. Geosci 8, 58. https://doi.org/10.3390/geosciences8020058.
Hejazi, M., Santos Da Silva, S.R., Miralles-Wilhelm, F., Kim, S., Kyle, P., Liu, Y., Clarke, L., 2023. Impacts of water scarcity on agricultural production and electricity generation in the Middle East and North Africa. Front. Environ. Sci. 11, 1082930. https://doi.org/10.3389/fenvs.2023.1082930.
Huang, J., Yu, H., Guan, X., Wang, G., Guo, R., 2016. Accelerated dryland expansion under climate change. Nat. Clim. Chang. 6, 166–171. https://doi.org/10.1038/nclimate2837.
Humphrey, V., Gudmundsson, L., Seneviratne, S.I., 2016. Assessing global water storage variability from GRACE: trends, seasonal cycle, sub-seasonal anomalies and extremes. Surv. Geophys. 37, 357–395. https://doi.org/10.1007/s10712-016-9367-1.
Hussain, D., Khan, A.A., Hassan, S.N.U., Naqvi, S.A.A., Jamil, A., 2021. A time series assessment of terrestrial water storage and its relationship with hydro-meteorological factors in Gilgit-Baltistan region using GRACE observation and GLDAS-Noah model. SN Appl. Sci. 3, 533. https://doi.org/10.1007/s42452-021-04525-4.
Jing, W., Zhao, X., Yao, L., Di, L., Yang, J., Li, Y., Zhou, C., 2020. Can terrestrial water storage dynamics be estimated from climate anomalies? Earth Space Sci. 7, e2019EA000959. https://doi.org/10.1029/2019EA000959.
Joodaki, G., Wahr, J., Swenson, S., 2014. Estimating the human contribution to groundwater depletion in the Middle East, from GRACE data, land surface models, and well observations. Water Resour. Res. 50 (3), 2679–2692. https://doi.org/10.1002/2013WR014633.
Khaki, M., Hoteit, I., 2021. Monitoring water storage decline over the Middle East. J. Hydrol. 603, 127166. https://doi.org/10.1016/j.jhydrol.2021.127166.
Khaki, M., Forootan, E., Kuhn, M., Awange, J., van Dijk, A.I., Schumacher, M., Sharifi, M. A., 2018. Determining water storage depletion within Iran by assimilating GRACE data into the W3RA hydrological model. Adv. Water Resour. 114, 1–18. https://doi.org/10.1016/j.advwatres.2018.02.008.
Khan, A.A., Li, X., 2025. Recent global snow cover trends using the MODIS dataset from 2000 to 2021. Remote Sens. Appl. Soc. Environ. 39, 101662. https://doi.org/10.1016/j.rsase.2025.101662.
Khorrami, B., Gunduz, O., 2021. An enhanced water storage deficit index (EWSDI) for drought detection using GRACE gravity estimates. J. Hydrol. 603, 126812. https://doi.org/10.1016/j.jhydrol.2021.126812.
Khorrami, B., Pirasteh, S., Ali, S., Sahin, O.G., Vaheddoost, B., 2023a. Statistical downscaling of GRACE TWSA estimates to a 1-km spatial resolution for a local-scale surveillance of flooding potential. J. Hydrol. 624, 129929. https://doi.org/10.1016/j.jhydrol.2023.129929.
Khorrami, B., Ali, S., Abadi, L.H., Jehanzaib, M., 2023b. Spatio-temporal variations in characteristics of terrestrial water storage and associated drought over different geographic regions of Türkiye. Earth Sci. Inf. 16, 717–731. https://doi.org/10.1007/s12145-022-00907-3.
Khorrami, B., Ali, S., Sahin, O.G., Gunduz, O., 2023c. Model-coupled GRACE-based analysis of hydrological dynamics of drying Lake Urmia and its basin. Hydrol. Process. 37, e14893. https://doi.org/10.1002/hyp.14893.
Khorrami, B., Gorjifard, S., Ali, S., Feizizadeh, B., 2023d. Local-scale monitoring of evapotranspiration based on downscaled GRACE observations and remotely sensed data: an application of terrestrial water balance approach. Earth Sci. Inf. https://doi.org/10.1007/s12145-023-00964-2.
Khorrami, B., Sahin, O.G., Gunduz, O., 2024. Comprehensive comparison of different gridded precipitation products over geographic regions of Türkiye. J. Appl. Remote. Sens. 18, 034503. https://doi.org/10.1117/1.JRS.18.034503.
Kim, H., Yeh, P.J.F., Oki, T., Kanae, S., 2009. Role of rivers in the seasonal variations of terrestrial water storage over global basins. Geophys. Res. Lett. 36, L17704. https://doi.org/10.1029/2009GL039006.
Konikow, L.F., Kendy, E., 2005. Groundwater depletion: a global problem. Hydrogeol. J. 13, 317–320. https://doi.org/10.1007/s10040-004-0411-8.
Krishnamurti, T.N., Pielke, R.A., Enfield, D.B., Loewe, F.P., Arnfield, A.J., Hayden, B.P., et al., 13 Sep. 2024. Climate. In: Encyclopedia Britannica. Accessed 14 Sep. 2024. https://www.britannica.com/science/climate-meteorology.
Lashkari, A., Irannezhad, M., Zare, H., Labzovskii, L., 2021. Assessing long-term spatio-temporal variability in humidity and drought in Iran using Pedj Drought Index (PDI). J. Arid Environ. 185, 104336. https://doi.org/10.1016/j.jaridenv.2020.104336.
Levine, P.A., Randerson, J.T., Swenson, S.C., Lawrence, D.M., 2016. Evaluating the strength of the land–atmosphere moisture feedback in earth system models using satellite observations. Hydrol. Earth Syst. Sci. 20, 4837–4856. https://doi.org/10.5194/hess-20-4837-2016.

Liu, J., Hull, V., Batistella, M., DeFries, R., Dietz, T., Fu, F., Zhu, C., 2013. Framing sustainability in a telecoupled world. Ecol. Soc. 18 (2). https://doi.org/10.5751/ES-05873-180226.

Longuevergne, L., Wilson, C.R., Scanlon, B.R., Crétaux, J.F., 2013. GRACE water storage estimates for the Middle East and other regions with significant reservoir and lake storage. Hydrol. Earth Syst. Sci. 17, 4817–4830. https://doi.org/10.5194/hess-17-4817-2013.

Mallick, J., Alqadhi, S., Talukdar, S., et al., 2025. Modeling GRACE-based groundwater drought and its teleconnections with global climate drivers for water sustainability in arid regions. Water Resour. Manag. https://doi.org/10.1007/s11269-025-04271-x.

Maxwell, R.M., Miller, N.L., 2005. Development of a coupled land surface and groundwater model. J. Hydrometeorol. 6, 233–247. https://doi.org/10.1175/JHM422.1.

McLeman, R., 2022. Developments in modelling of climate change-related migration. Clim. Chang. 117, 599–611. https://doi.org/10.1007/s10584-012-0578-2.

Mo, X., Wu, J.J., Wang, Q., Zhou, H.J.N., 2016. Variations in water storage in China over recent decades from GRACE observations and GLDAS. Nat. Hazards Earth Syst. Sci. 16, 469–482. https://doi.org/10.5194/nhess-16-469-2016.

Muhammad, A.S., Al-Mimar, H., Mundher, Y.Z., 2021. Groundwater availability and water demand sustainability over the upper mega aquifers of Arabian Peninsula and west region of Iraq. Environ. Dev. Sustain. 23, 1–21. https://doi.org/10.1007/s10668-019-00578-z.

Nikraftar, Z., Parizi, E., Saber, M., Hosseini, S.M., Ataie-Ashtiani, B., Simmons, C.T., 2024. Groundwater sustainability assessment in the Middle East using GRACE/GRACE-FO data. Hydrogeol. J. 32, 321–337. https://doi.org/10.1007/s10040-023-02717-3.

Paca, V.H.d.M., Espinoza-Dávalos, G.E., Moreira, D.M., Comair, G., 2020. Variability of trends in precipitation across the Amazon River Basin determined from the CHIRPS precipitation product and from station records. Water 12, 1244. https://doi.org/10.3390/w12051244.

Pokhrel, Y., Felfelani, F., Satoh, Y., Boulange, J., Burek, P., Gädeke, A., et al., 2021. Global terrestrial water storage and drought severity under climate change. Nat. Clim. Chang. 11, 226–233. https://doi.org/10.1038/s41558-020-00972-w.

Rezaee, A., Mosaedi, A., Beheshti, A., et al., 2024. Using wavelet transform to analyze the dynamics of climatic variables; to assess the status of available water resources in Iran (1961–2020). Earth Sci. Inf. 17, 5499–5519. https://doi.org/10.1007/s12145-024-01433-0.

Rodell, M., Famiglietti, J.S., 2001. An analysis of terrestrial water storage variations in Illinois with implications for the Gravity Recovery and Climate Experiment (GRACE). Water Resour. Res. 37, 1327–1339. https://doi.org/10.1029/2000WR900306.

Rodell, M., Houser, P.R., Jambor, U., Gottschalck, J., Mitchell, K., Meng, C.-J., Arsenault, K., Cosgrove, B., Radakovich, J., Bosilovich, M., Entin, J.K., Walker, J.P., Lohmann, D., Toll, D., 2004. The Global Land Data Assimilation System. Bull. Am. Meteorol. Soc. 85, 381–394. https://doi.org/10.1175/BAMS-85-3-381.

Rousta, I., Olafsson, H., Moniruzzaman, M., Zhang, H., Liou, Y.A., Mushore, T.D., Gupta, A., 2020. Impacts of drought on vegetation assessed by vegetation indices and meteorological factors in Afghanistan. Remote Sens. 12, 2433. https://doi.org/10.3390/rs12152433.

Scanlon, B.R., Faunt, C.C., Longuevergne, L., Reedy, R.C., Alley, W.M., McGuire, V.L., McMahon, P.B., 2012a. Groundwater depletion and sustainability of irrigation in the US High Plains and Central Valley. Proc. Natl. Acad. Sci. USA 109, 9320–9325. https://doi.org/10.1073/pnas.1200311109.

Scanlon, B.R., Faunt, C.C., Longuevergne, L., Reedy, R.C., Alley, W.M., McGuire, V.L., McMahon, P.B., 2012b. Groundwater depletion and sustainability of irrigation in the US High Plains and Central Valley. Proc. Natl. Acad. Sci. 109 (24), 9320–9325. https://doi.org/10.1073/pnas.1200311109.

Scanlon, B.R., Zhang, Z., Save, H., Wiese, D.N., Landerer, F.W., Long, D., et al., 2016. Global evaluation of new GRACE mascon products for hydrologic applications. Water Resour. Res. 52, 9412–9429. https://doi.org/10.1002/2016WR019494.

Water resources in the Middle East. In: Shaban, A. (Ed.), 2022. Satellite Monitoring of Water Resources in the Middle East. Springer, pp. 15–17. https://doi.org/10.1007/978-3-031-15549-9.

Shrestha, P., Sulis, M., Masbou, M., Kollet, S., Simmer, C., 2014. A scale-consistent terrestrial systems modelling platform based on Cosmo, CLM, and Parflow. Mon. Weather Rev. 142, 3466–3483. https://doi.org/10.1175/MWR-D-14-00029.1.

Soltani, S.S., Ataie-Ashtiani, B., Danesh-Yazdi, M., Simmons, C.T., 2020. A probabilistic framework for water budget estimation in low runoff regions: a case study of the central basin of Iran. J. Hydrol. 586, 124898. https://doi.org/10.1016/j.jhydrol.2020.124898.

Soltani, S.S., Ataie-Ashtiani, B., Simmons, C.T., 2021. Review of assimilating GRACE terrestrial water storage data into hydrological models: advances, challenges and opportunities. Earth Sci. Rev. 213, 103487. https://doi.org/10.1016/j.earscirev.2020.103487.

Soltani, S.S., Fahs, M., Al Bitar, A., Ataie-Ashtiani, B., 2022. Improvement of soil moisture and groundwater level estimations using a scale-consistent river parameterization for the coupled ParFlow-CLM hydrological model: a case study of the Upper Rhine Basin. J. Hydrol. 610, 127991. https://doi.org/10.1016/j.jhydrol.2022.127991.

Soltani, S.S., Ataie-Ashtiani, B., Al Bitar, A., Simmons, C.T., Younes, A., Fahs, M., 2024. Assimilating multivariate remote sensing data into a fully coupled subsurface-land surface hydrological model. J. Hydrol. 131812. https://doi.org/10.1016/j.jhydrol.2024.131812.

Sun, G., Vose, J.M., 2016. Forest management challenges for sustaining water resources in the Anthropocene. Forests 7 (3), 68. https://doi.org/10.3390/f7030068.

Syed, T.H., Famiglietti, J.S., Rodell, M., Chen, J., Wilson, C.R., 2008. Analysis of terrestrial water storage changes from GRACE and GLDAS. Water Resour. Res. 44 (2). https://doi.org/10.1029/2006WR005779.

Syed, F.S., Adnan, S., Zamreeq, A., Ghulam, A., 2022. Identification of droughts over Saudi Arabia and global teleconnections. Nat. Hazards 112 (3), 2717–2737. https://doi.org/10.1007/s11069-022-05285-z.

Tapley, B.D., Watkins, M.M., Flechtner, F., Reigber, C., Bettadpur, S., Rodell, M., Velicogna, I., 2019. Contributions of GRACE to understanding climate change. Nat. Clim. Chang. 9 (5), 358–369. https://doi.org/10.1038/s41558-019-0456-2.

Torrence, C., Compo, G.P., 1998. A practical guide to wavelet analysis. Bull. Am. Meteorol. Soc. 79, 61–78. https://doi.org/10.1175/1520-0477(1998)079<0061:APGTWA>2.0.CO;2.

Vaheddoost, B., Mohammadi, B., 2025. A study of the relationship between GRACE-TWSA and large-scale atmospheric-oceanic patterns. Hydrol. Sci. J. https://doi.org/10.1080/02626667.2025.2537851.

Voss, K.A., Famiglietti, J.S., Lo, M., De Linage, C., Rodell, M., Swenson, S.C., 2013. Groundwater depletion in the Middle East from GRACE with implications for transboundary water management in the Tigris-Euphrates-Western Iran region. Water Resour. Res. 49 (2), 904–914. https://doi.org/10.1002/wrcr.20078.

Walther, B.A., Huettmann, F., 2021. Palearctic passerine migrant declines in African wintering grounds in the Anthropocene (1970–1990 and near future): a conservation assessment using publicly available GIS predictors and machine learning. Sci. Total Environ. 777, 146093. https://doi.org/10.1016/j.scitotenv.2021.146093.

Wang, S., Cui, G., Li, X., Liu, Y., Li, X., Tong, S., Zhang, M., 2023. GRACE satellite-based analysis of spatiotemporal evolution and driving factors of groundwater storage in the Black Soil Region of Northeast China. Remote Sens. 15, 704. https://doi.org/10.3390/rs15030704.

Wasko, C., Nathan, R., Peel, M.C., 2020. Trends in global flood and streamflow timing based on local water year. Water Resour. Res. 56. https://doi.org/10.1029/2020WR027233 e2020WR027233.

Xiong, J., Yang, Y., 2025. Climate change and hydrological extremes. Curr. Clim. Chang. Rep. 11, 1. https://doi.org/10.1007/s40641-024-00198-4.

Yang, Y., Roderick, M.L., Zhang, S., McVicar, T.R., Donohue, R.J., 2019. Hydrologic implications of vegetation response to elevated CO2 in climate projections. Nat. Clim. Chang. 9 (1), 44–48. https://doi.org/10.1038/s41558-018-0361-0.

Yang, X., Wang, N., Liang, Q., Chen, A.A., Wu, Y., 2021. Impacts of human activities on the variations in terrestrial water storage of the Aral Sea basin. Remote Sens. 13 (15), 2923. https://doi.org/10.3390/rs13152923.

Yassin, M.A., Abba, S.I., Pradipta, A., Makkawi, M.H., Shah, S.M.H., Usman, J., Sammen, S.S., 2024. Advancing SDGs: predicting future shifts in Saudi Arabia's terrestrial water storage using multi-step-ahead machine learning based on GRACE data. Water 16 (2), 246. https://doi.org/10.3390/w16020246.

Yin, J., Gentine, P., Slater, L., Gu, L., Pokhrel, Y., Hanasaki, N., Schlenker, W., 2023. Future socio-ecosystem productivity threatened by compound drought–heatwave events. Nat. Sustainability 6 (3), 259–272. https://doi.org/10.1038/s41893-022-01024-1.

Youssefi, F., Soltani, S.S., Ali, S., Khorrami, B., 2025. Integrating fully-coupled hydrological modeling and random forest to enhance spatial resolution of GRACE-observed water storage across the Rhine Basin. Nat. Resour. Res. 34, 2667–2684. https://doi.org/10.1007/s11053-025-10528-4.

Zhang, Y., He, B., Guo, L., Liu, J., Xie, X., 2019. The relative contributions of precipitation, evapotranspiration, and runoff to terrestrial water storage changes across 168 river basins. J. Hydrol. 579, 124194. https://doi.org/10.1016/j.jhydrol.2019.124194.

Zhang, G., Xu, T., Yin, W., Bateni, S.M., Jun, C., Kim, D., Wang, J., 2024. A machine learning downscaling framework based on a physically constrained sliding window technique for improving resolution of global water storage anomaly. Remote Sens. Environ. 313, 114359. https://doi.org/10.1016/j.rse.2024.114359.

Zhao, F., Ma, S., Wu, Y., 2021. Changes in dry-season water availability and attributions in the Yellow River Basin, China. Front. Environ. Sci. 9, 762137. https://doi.org/10.3389/fenvs.2021.762137.

Zhong, Y., Zhong, M., Mao, Y., Ji, B., 2020. Evaluation of evapotranspiration for exorheic catchments of China during the GRACE era: from a water balance perspective. Remote Sens. 12 (3), 511. https://doi.org/10.3390/rs12030511.

Zomer, R.J., Xu, J., Trabuco, A., 2022. Version 3 of the global aridity index and potential evapotranspiration database. Sci. Data 9, 409. https://www.nature.com/articles/s41597-022-01493-1.